OPERATIONS, ACCELERATOR PHYSICS, AND INSTRUMENTATION

K1200 OPERATING EXPERIENCE

D.R. Poe, H.A. Thulin, M. Garbek and P.S. Miller

Table I shows operating time statistics for the K1200 cyclotron in 1994, and Table II shows the various beams which were run. There were 82 beams with 108 different beam changes in 5211.25 hours of operation, and 3864.75 hours of research. This means that there was a beam change every 48.25 hours of operation and every 35.78 hours of research time.

TABLE I K1200 Time Distribution 1994

Operation	Hours	Percentage
Research	3864.75	63.38
Development	454.50	7.45
Overhead	892.00	14.63
R + D + O	5211.25	85.46
Maintenance	269.75	4.42
Breakdown	616.75	10.12
TOTAL	6097.75	100.00
Off	2588.25	
Startup	74.00	

EFFICIENCY = E = (R + D + O) / (TOTAL - Maintenance)
E = 5211.25 / (6097.75 - 269.75) = 0.894 = 89.4 %

There were 3864.75 hours of research time in 1994 against 5102.25 hours in 1993. This reflects the greater amount of off time in 1994, 2588.25 versus 1425.75, due to the long shutdown starting in February. The category of operation, or research + development + overhead, which represents the time that the cyclotron was running, was 5211.25 hours in 1994. The efficiency as defined in Table I, which is the time the cyclotron ran divided by the time that we tried to run it, decreased from 90.8 % to 89.4 %.

The total number of hours in 1994 was 8760. Research was therefore carried on 44.1% of the time and operation 59.4%.

On February 2, 1994, a beam of 200 MeV/u $^{16}O^{8+}$ was first extracted from the cyclotron. In order to accomplish this, the coil was raised relative to the yoke 0.025 inches (0.6 mm), after which the beam had adequate vertical stability to allow it to survive on the median plane to extraction radius.

As was noted last year, the dee stems are now using silicone rubber O-rings. (The original indium seals would not last, and Delta seals did not work.) This seems to be a success, but there is concern that the slight diffusion of air through the O-rings is degrading the vacuum. Finding better O-ring materials, which stand up to the harsh RF conditions over time but are better vacuum materials, is an ongoing project at this time.

The hydraulic drivers for the input coupling capacitors, which couple RF power into the dees, have been replaced with electric motors in an effort to improve reliability.

The K1200 cyclotron was raised vertically 0.2 inches in February so as to provide better alignment with the A1200 and beamline. The cyclotron was raised with hydraulic jacks at the support posts, inserting shims at each support post in turn, after all necessary equipment was disconnected.

TABLE II K1200 BEAMS 1994

ION	E/A (MeV)	Hours	% Time
$^{2}H_{2}^{1+}$	200	12.3	0.3
$^{2}H_{2}^{1+}$	155	36.0	0.8
$^{3}(H\text{-}D)^{1+}$	100	34.3	0.8
$^{3}(H\text{-}D)^{1+}$	70	12.3	0.3
$^{4}He^{2+}$	200	11.8	0.3
$^{4}He^{2+}$	155	51.8	1.2
$^{4}He^{1+}$	40	22.0	0.5
$^{5}(H\text{-}He)^{1+}$	35	32.0	0.7
$^{6}Li^{2+}$	65	80.8	1.9
$^{6}Li^{1+}$	22	3.0	0.1
$^{7}Li^{2+}$	90	149.5	3.5
$^{7}Li^{2+}$	70	126.3	3.0
$^{7}Li^{2+}$	50	110.5	2.6
$^{12}C^{6+}$	200	0.8	0.0
$^{12}C^{6+}$	155	6.0	0.1
$^{12}C^{4+}$	100	1.5	0.0
$^{12}C^{3+}$	40	19.5	0.5
$^{12}C^{2+}$	22	116.8	2.7
$^{12}N^{5+}$	125	3.0	0.1
$^{14}N^{6+}$	120	203.5	4.8
$^{14}N^{4+}$	90	8.8	0.2
$^{16}O^{8+}$	200	32.8	0.8
$^{16}O^{8+}$	170	2.0	0.0
$^{16}O^{8+}$	155	40.8	1.0
$^{16}O^{7+}$	150	5.0	0.1
$^{16}O^{5+}$	100	2.5	0.1
$^{16}O^{6+}$	80	127.8	3.0
$^{16}O^{4+}$	60	283.5	6.6
$^{16}O^{4+}$	40	27.5	0.6
$^{18}O^{6+}$	80	23.8	0.6
$^{18}O^{3+}$	22	22.0	0.5
$^{20}Ne^{6+}$	100	12.0	0.3
$^{22}Ne^{4+}$	35	0.5	0.0
$^{36}Ar^{17+}$	160	232.8	5.4
$^{36}Ar^{12+}$	100	36.8	0.9
$^{36}Ar^{6+}$	22	55.8	1.3
$^{40}Ar^{12+}$	100	97.8	2.3
$^{40}Ar^{12+}$	90	90.3	2.1
$^{40}Ar^{12+}$	80	110.3	2.6
$^{40}Ar^{10+}$	60	29.3	0.7
$^{40}Ar^{10+}$	40	39.0	0.9
$^{40}Ca^{8+}$	35	160.0	3.7
$^{48}Ca^{10+}$	35	45.8	1.1
$^{55}Mn^{14+}$	70	89.8	2.1
$^{58}Ni^{15+}$	70	107.0	2.5
$^{78}Kr^{22+}$	75	62.0	1.5
$^{81}Kr^{17+}$	45	77.3	1.8
$^{84}Kr^{30+}$	125	4.0	0.1
$^{84}Kr^{21+}$	60	1.5	0.0
$^{86}Kr^{26+}$	100	75.5	1.8
$^{86}Kr^{26+}$	95	9.8	0.2
$^{86}Kr^{25+}$	85	22.0	0.5
$^{86}Kr^{22+}$	70	5.8	0.1
$^{86}Kr^{22+}$	65	77.3	1.8
$^{86}Kr^{19+}$	50	116.5	2.7
$^{86}Kr^{19+}$	45	4.5	0.1
$^{86}Kr^{18+}$	45	18.3	0.4
$^{86}Kr^{18+}$	35	3.0	0.1
$^{86}Kr^{16+}$	35	151.0	3.5
$^{86}Kr^{15+}$	30	35.8	0.8
$^{86}Kr^{15+}$	25	15.3	0.4
$^{93}Nb^{21+}$	50	16.8	0.4
$^{112}Sn^{22+}$	40	2.0	0.0
$^{124}Sn^{25+}$	40	3.0	0.1
$^{129}Xe^{40+}$	100	8.5	0.2
$^{129}Xe^{31+}$	65	75.5	1.8
$^{129}Xe^{30+}$	60	15.5	0.4
$^{129}Xe^{27+}$	45	10.0	0.2
$^{129}Xe^{25+}$	40	2.0	0.0
$^{129}Xe^{26+}$	40	39.3	0.9
$^{129}Xe^{23+}$	30	35.5	0.8
$^{129}Xe^{19+}$	20	53.5	1.3
$^{136}Xe^{25+}$	35	7.8	0.2
$^{136}Xe^{24+}$	30	29.5	0.5
$^{197}Au^{41+}$	45	10.0	0.2
$^{197}Au^{38+}$	40	87.5	2.0
$^{197}Au^{36+}$	35	103.5	2.4
$^{197}Au^{34+}$	30	92.0	2.2
$^{197}Au^{32+}$	25	86.3	2.0
$^{197}Au^{29+}$	20	17.5	0.4
$^{238}U^{35+}$	20	127.5	3.0
Total		4275.3	100.0

During the shutdown when the cylotron was raised, the singlet and doublet quadrupole magnets immediately outside of the K1200 were moved to provide better matching into the beamline. At the same time, the fields in the yoke midplane and immediately outside were measured and compared to TOSCA results to formulate discrepancies, and a ray tracing program was written to track particles

through the region. The result allows ray tracing to be incorporated in the routine beam calculations, with improved matching into the beamline.

Deflectors are now able to run up to 120 kV/cm operationally, or 72 kV, and we have had tests at 80 kV with a few days of beam time there.

Efforts are underway to improve the cooling of the deflectors, since a major limiting factor seems to be beam power. We are attempting to provide cooling to the high voltage feedthroughs, and we are trying to make shoe insulators out of materials more conductive of heat, for example beryllium oxide and aluminum nitride.

REPOSITIONING OF THE K1200 CYCLOTRON

D. Johnson, D. Lawton, F. Marti, P. Miller, D. Poe, D. Sanderson, J. Stetson, and C. Snow

In February 1994 the K1200 cyclotron was raised 0.2 inch to match its median plane to that of the beam lines in the A1200 and the experimental areas. The vertical and horizontal positions of the quadrupoles in the cyclotron vault were also adjusted to match the predicted path of the extracted beam from the cyclotron to the A1200. Some benchmarks were placed in the cyclotron vault, and a survey was performed to measure the location of the cyclotron center in the building coordinate system. To do this, a stable mounting base for the transit was installed permanently on the north side of the K1200 vault, where the center axis of the cyclotron could be seen through access port A1. A reference point on the beam line was also measured from this position.

Vertical position

For some time before the cyclotron shutdown the position and spot size of the beam at scintillators A-12SC ("Pot 0", Cyclotron exit) and A-04FR("Pot 1", 95 inches downstream) were measured routinely as each beam was developed. These data were analyzed to determine the emittance and displacement of the beam. The position of the beam (with zero currents in the quadrupoles) was 6 to 12 mm (0.24 to 0.47 inch) below the center of the scintillator at Pot 0 and 5 to 13 mm (0.20 to 0.51 inch) below the center at Pot 1. We concluded that the beam was exiting the cyclotron below the beam line center and was approximately level. The relative altitudes of the cyclotron and some points on the beam line were compared using a water level. This device had a precision of ±2 mm (.08 inch). It indicated that the cyclotron was approximately 0.3 inch below the center of the A1200 beam line, and the quadrupoles in the cyclotron vault (A-10QS, A-08QA and A-06QB) were approximately 0.1 inch *above* it. (see Fig. 1). Later measurements with a transit installed in the beam line after a wall was removed showed that the cyclotron was 0.206 inch below the desired level.

In the week before the 2 month shutdown when the repositioning was done the K1200 main magnet coil was moved vertically, as part of the development of a 200 MeV/u beam. This coil movement (net: 0.025 inch upward) turned out to be essential for stable vertical motion of the beam to extraction. The effect of this coil shift on the position and direction of the external beam is uncertain. We now observe that the beam just outside the cyclotron is sloping upward. We do not have a vertical corrector between the first 3 quadrupoles and the cyclotron. It is therefore necessary to make the first singlet vertically focusing and to steer the beam with it. Although optics solutions with the first singlet horizontally focusing are theoretically valid they are not practical because of the vertical alignment constraint.

Before the magnet was raised a number of subsystems had to be disconnected or checked for sufficient movement capability. On the upper pole cap these were: magnet power and instrument leads, magnet cryogenic lines, helium vent pipe, resonator air and RF cable trays, and RF dee stem drives. On the return path rings these were: floor plates and probe drives. On the lower pole cap these were: trim coil bus bars, RF transmission lines, resonator air delivery, pole lowering system, water manifold system, floor plates, cryopump distribution, and injection beam line supports. The magnet was supported on 3 round steel columns. It was raised by jacking the magnet on one column at a time and inserting shims. The maximum horizontal deflection of the upper dee stems from the resulting tilt was 0.56 inch. Two shims (0.118 and 0.088 inch thick) totaling 0.206 inch thickness were added to each column. After shimming, the height of the cyclotron was 0.004 inch below the A1200 reference height.

The hydraulic jack used had to lift one third of the weight of the cyclotron. The weight of the

cyclotron was indicated by the jack pressure gauge to be 350 tons (US). When the jack was calibrated in another experiment against a load cell the gauge was found to be reading 84% of the actual weight. The corrected weight of the cyclotron is therefore 417 tons.

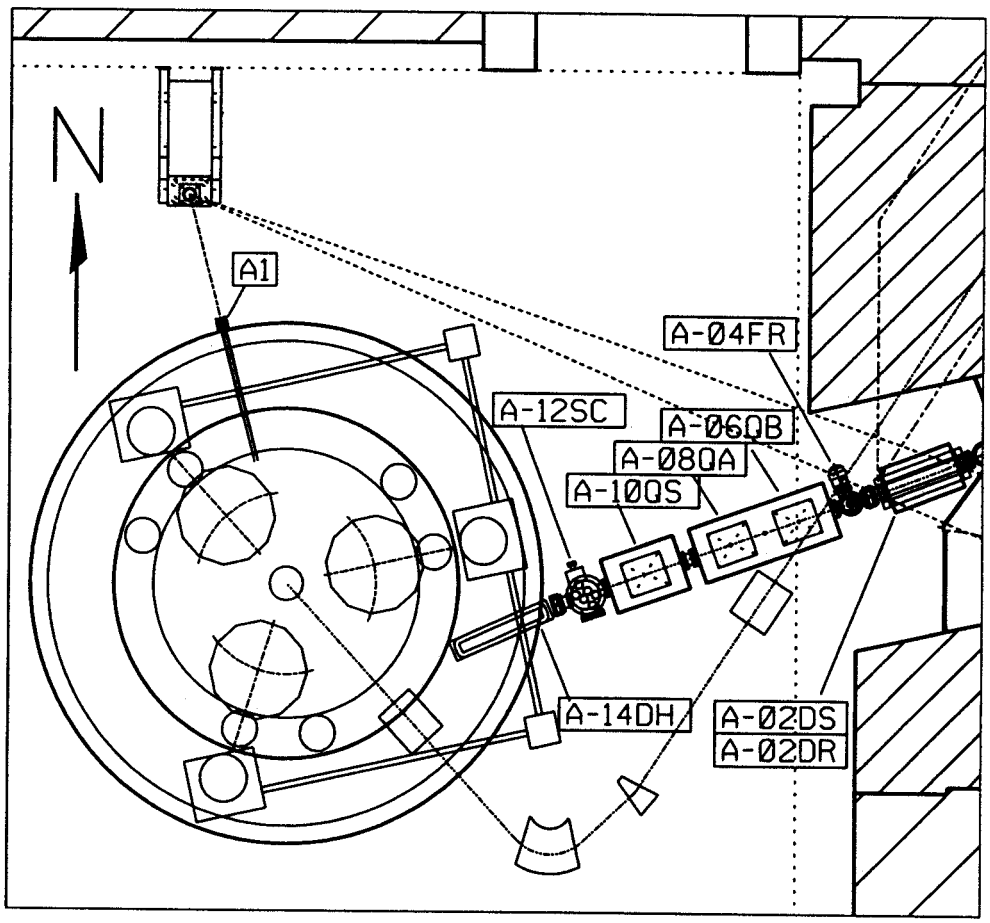

Figure 1: Plan view showing K1200 cyclotron, beam line and transit support.

Horizontal alignment of the cyclotron beam to the beam line

Before the quadrupoles were repositioned, the beam was observed to be 6 to 13 mm (0.24 to 0.51 inch) south of center at Pot 0 (i.e. to the right, looking downstream) when adjusted to minimize steering effects from the quads. The positions of Pot 0, Pot 1 and flanges of beamline magnets were marked on the floor with a plumb line and their coordinates were determined. A consistent picture emerged, that the singlet and doublet were aligned to an axis that was rotated too far south. The center of Pot 0 was north of this axis. To make the beam pass near the quadrupole axis one had to aim it near the south edge of the entrance aperture of the exit dipole. The nominal center of the beam aperture at the matching point for transition from cyclotron to beam line was R=53.12 inches at theta=356 deg. In order to get reasonable beam matching we had been using a matching radius 0.5 inch larger. This caused the beam to graze the south side of the aperture at the entrance to the exit dipole. We proceeded to calculate, and later to measure, the magnetic field in the yoke of the cyclotron magnet and trace rays from the cyclotron to the beam line. The intended strategy for matching was to use the position at the matching point (the "ΔR" value) and the exit dipole current as adjustable parameters to align the beam to the quadrupole axis.

Magnetic field in the yoke and external to the yoke

We calculated the magnetic field with TOSCA[1] using a magnet model that had been prepared to study injection of beam into the K1200. Discrepancies between calculated and observed beam positions could not be resolved, so the field was measured in the midplane through the exit dipole and outside the yoke. A systematic discrepancy which varied smoothly with the magnet excitation was discovered. The difference between the field calculated and field measured was a linear function of a particular combination of magnet currents: $I_a + 0.47979\ I_b$. This discrepancy is attributed to the sensitivity of the calculation to the mesh size and the complex shape of the iron components. It was then possible to determine the correction to the field from TOSCA for any magnet currents. The field was mapped at 11 excitations of the magnet. A program was written (INJORBEX4) to give the field at any other currents by interpolation in the measured maps, and to find the particle starting coordinate and momentum and dipole current (A-14DH) to yield the ray on the quadrupole axis (see Fig. 2). The coordinate system (xline, yline) is rotated to place the xline-axis nearly coincident with the beam path from cyclotron to the dipole magnet A-02DS. The trajectories shown in Fig. 2 are for 9 different ion/energy cases covering the operating range of the cyclotron. The quadrupoles are aligned on the dashed line connecting two diamond shaped points. The goal of the procedure is to have the trajectories coincide with this line. The width of the entrance and exit apertures of the exit dipole, A-14DH, is indicated by the two error bars. All the rays shown remain clear of these apertures with a margin for the beam envelope.

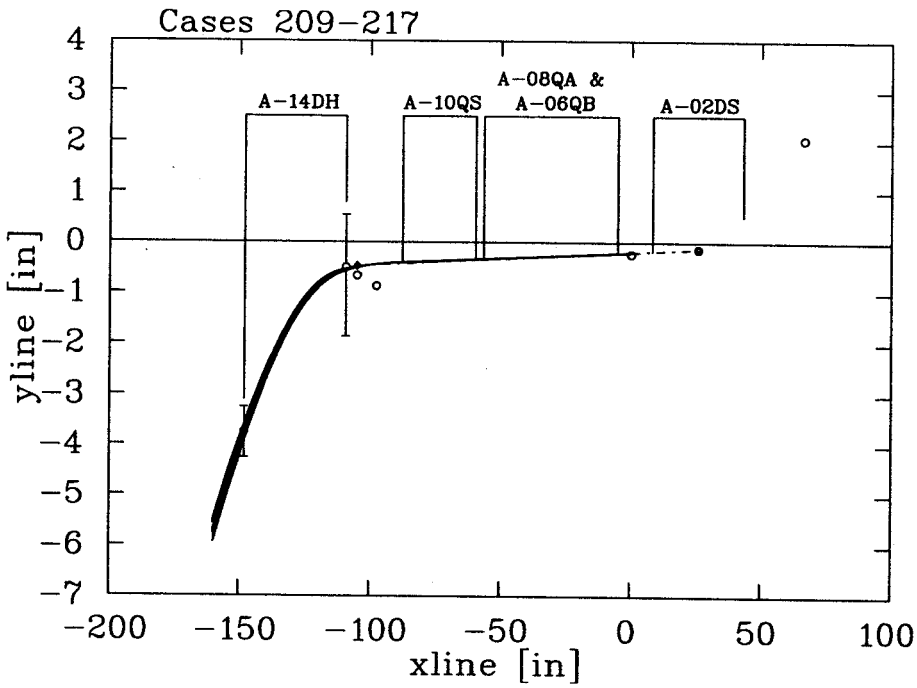

Figure 2: Trajectories predicted by INJORBEX4

The measured fringe field of the cyclotron in the quadrupoles is very low. We use the approximation that the field is zero from the entrance of the first quadrupole onward.

The exit dipole power supply (400 A max.) was replaced with a 500 A supply to handle the anticipated increase in bending required. A water booster pump for the dipole coil was added. It is controlled automatically by water temperature, so the temperature is always less than the previous maximum at 400 A (151 F). The pump starts at 150 F and stops at 110 F.

Results

The beam is horizontally centered in the exit dipole aperture with a margin for moving it during beam line tuning. The beam is tuned by a prescription that is based on experience with minimizing steering by the quadrupoles and preserving the essential parameters of the optical solution for the beam line. The exit dipole field is set at the value from an empirical formula. The horizontal position of the beam is adjusted by means of focusing bar positions to about 4 mm south of center at Pot 0.

As stated above, the remaining vertical mismatch forces the quadrupoles to steer. This could be improved by adding a vertical correcting magnet ahead of or incorporated into the first quadrupole. When this element is available it may be possible to implement a strategy of aligning the beam independently of the strength of quadrupoles.

Reference

1. Vector Fields, Inc.

PROPOSED UPGRADE OF THE NSCL

R.C. York, H. Blosser, T. Grimm, D. Johnson, D. Lawton, F. Marti, J. Vincent, X. Wu, and A.F. Zeller

The present nuclear physics program at the National Superconducting Cyclotron Laboratory (NSCL) is based on an ECR-ion-source-injected K1200 superconducting cyclotron. We propose to significantly increase the facility's output intensity for light ions and energy for heavy ions by coupling the existing superconducting K500 cyclotron's output to the K1200. The improved acceleration chain will consist of an ECR-ion-source-injected K500 cyclotron to accelerate ions to $\leq$17 MeV/nucleon followed by radial, charge-stripping injection into the K1200 for final acceleration to 100-200 MeV/nucleon.

Introduction

The NSCL proposes to couple its two superconducting cyclotrons (K500 and K1200) and to replace the existing fragment separator (A1200) with one of increased capacity (A1900) as shown in Figure 1. Since the upgrade relies on the existing cyclotrons and incorporates the present experimental facilities, it can proceed in a timely (~4 - 5 years estimated project duration) and cost-effective fashion (~ 19M FY94 US$ in total project costs including labor and materials).

The coupling of the cyclotrons (K500⊗K1200) will provide significant increases in the primary beam intensity and for the heaviest ions, in beam energy permitting a wide variety of experimental programs to be undertaken which are presently not feasible.

Performance

The maximum theoretically achievable energy is determined by the characteristics of the K1200 cyclotron. The improvements in energy and intensity that come with coupling the cyclotrons result from the lower charge states required from the ECR ion source for the K500⊗K1200 mode. These lower charge states needed from the ECR to achieve the same final energy have significantly more intensity than the higher K1200 stand-alone charge states.[1]

Large gains in intensity are possible for all ions considered, and in addition, there are significant gains in energy for mid and high-mass nuclei. Figure 2 shows these gains and also illustrates the possible trade-off of intensity for energy. Shown are contours of intensity as a function of E/A and A for the K500⊗K1200 operation (solid lines) and the present K1200 stand-alone operation (dashed lines). The intensities are also given at specific points for the K500⊗K1200 operation (solid) and stand-alone operation (open). For heavier beams, the intensity gains for highly charged ions effectively result in higher energy beams (by factors of 2 - 4). Note that energies of over 100 MeV/nucleon are possible for uranium, while intensities up to 6×10^{12} particles/s are possible for lighter ions.

The greater intensities for the lighter ions are an excellent match to the needs of the growing field of nuclear physics research using radioactive ion beams, as they can be converted into very intense, good-quality secondary beams. To fully capitalize upon the increased primary beam intensities for the production of secondary radioactive beams, a large projectile-fragment separator (A1900) is proposed. In order to produce and separate rigid neutron-rich nuclei at optimal production energies, the A1900 will have ~30% greater bending power than that of the cyclotron (K1200), and will have a collection efficiency for fragmentation products approaching 50% compared to the 2-4% for the present NSCL system (A1200). Intensities for some representative ions are given in Table 1.

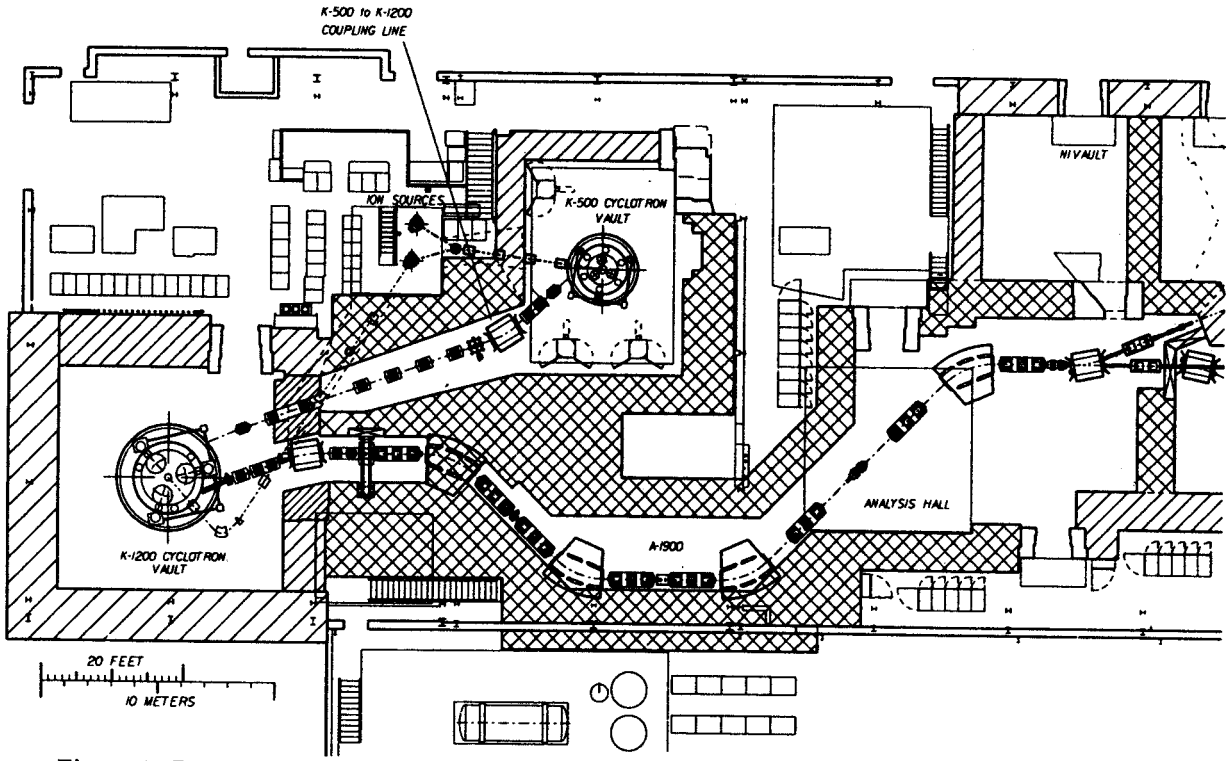

Figure 1: Proposed new accelerator area of the National Superconducting Cyclotron Laboratory.

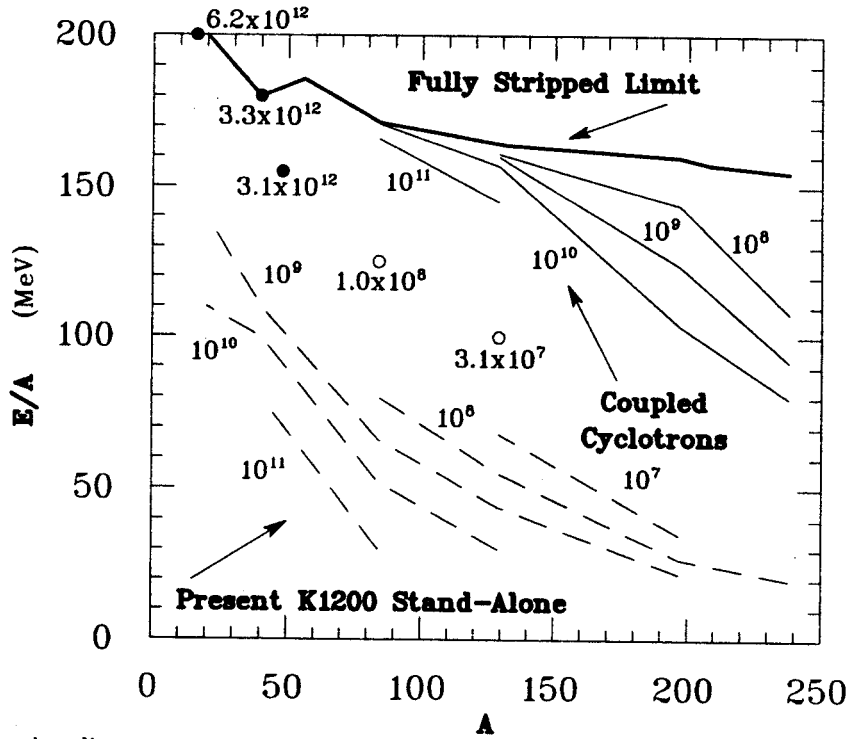

Figure 2: Operating diagram for the present K1200 stand-alone cyclotron and the K500⊗K1200 system. Intensity contours in particles per second are given for the K1200 stand-alone cyclotron (dashed) and the K500⊗K1200 (solid). The intensity is also given at specific points for the K1200 stand-alone (open) and the K500⊗K1200 (solid) operation. The present K1200 stand-alone performance contours are based upon the performance of the room temperature ECR with specific points (open) based upon the superconducting ECR performance.

	^{11}Li	^{19}Ne	^{32}Mg	^{56}Ni	^{132}Sn
K1200 & A1200	2.5×10^{3}	6×10^{7}	1.2×10^{3}	7×10^{4}	2
K500⊗K1200 & A1900	4×10^{6}	1×10^{10}	3×10^{6}	1×10^{8}	4×10^{4}

Table 1: Intensities (ions/sec) of representative radioactive beams achievable with K1200 stand-alone operation compared to those predicted for the K500⊗K1200 coupled cyclotron operation using the A1900 fragment separator.

Design

Some parameter details for the injection chain are given in Table 2. Ions of charge state Q_1 will be produced in an ECR ion source, transported from the ion source area to a point below the K500 and axially injected into the K500 central region. Ion intensities of $\sim 10^{13}$ particles/s will be accelerated in the K500 in approximately 230 turns to energies of $\leq$ 17 MeV/u. The beams will then be transported to the K1200 with a system of magnetic elements and an rf system (used to control the bunch length between the two cyclotrons) and injected through an existing horizontal port to a point at approximately one third of the K1200 extraction radius (~0.33 m) where they will be stripped to a higher charge state Q_2. Finally, the beam of charge state Q_2 will be accelerated in the K1200 to final energies of $\leq$200 MeV/u and extracted. Following the K1200, the extracted beam will be optically matched to a new beam analysis system, the A1900. As with the present A1200 analysis system, the A1900 will be positioned as the first element of the switch yard so that any beam, including separated fragments, can be delivered to any of the experimental areas.

	K500		Strip.	K1200		
Ion	Q_1	Energy (MeV/u)	Effic. %	Q_2	Energy (MeV/u)	Intensity (part./s)
^{16}O	3	16.7	100	8	200	6.2×10^{12}
^{84}Kr	15	14.7	2.2	36	170	2.1×10^{10}
^{238}U	32	8.6	2	74	90	1.2×10^{9}

Table 2: K500⊗K1200 parameter details for selected ions.

Project scope

The operating voltage of the existing superconducting and room temperature ECR ion sources will be increased from $\sim$ 20 kV to $\sim$ 30 kV in order to mitigate space charge effects, increase the beam brightness, and reduce the deleterious effects of the K500 fringe fields on the injection process. The existing coupling line between the K500 and the ECR ion sources will be modified in order to provide for efficient transport of high intensity beams.

The K500 cyclotron will be refurbished to obtain the operating reliability which is currently achieved by the K1200 cyclotron (>90%). During the refurbishing process, the K500 will be disassembled with reassembly in a position rotated 120° from its present position to orient the extraction channel towards the K1200. In addition to the implementation of proven K1200-like engineering solutions, a

Task	Funding Required (FY94 M$)
ECR/Injection Upgrade	0.50
K500 Upgrade	3.08
Coupling Line	2.11
K1200 Upgrade	1.29
A1900	4.46
Building Systems Upgrades	3.67
Commissioning	0.15
Total	15.26
Contingency (~25%)	3.68
Grand Total	18.94

Table 3: K500⊗K1200 Costs in FY94 M$.

new central region will be used to allow more efficient operation at the second harmonic and a higher performance extraction septum will be installed.

A new coupling line between the K500 and the K1200 will be implemented. In the K1200, the injection hardware will be installed and the extraction hardware improved. (The capability to operate the K1200 cyclotron in the stand-alone mode will be retained.) The present fragment separator (A1200) will be replaced with a much higher performance system (A1900).

The NSCL high bay area will be extended by approximately 25 m in order to provide a staging area for magnet construction and refurbishing of the K500. A building addition will be constructed near the present cryogenic plant to house a cryogenic system of increased capacity, and the radiation shielding will be increased.

The total project costs are given in Table 3.

Present status

The design concept for the K500⊗K1200 was developed during 1993-1994. A conceptual design report was published [2] and a proposal was submitted to the National Science Foundation (NSF) in 1994 in which a cost sharing strategy between Michigan State University (8 FY94 M$) and NSF (11 FY94 M$) was specified. Since that time, research and development projects have begun on certain aspects of the design. MSU has already committed a portion of its contribution (~ 1 M$) for the extension of the high bay area with construction scheduled for completion near the end of 1995.

Detailed design and initial prototyping of programmatic elements such as the coupling line rf system and the stripping foil system to be used in the K1200 are in process.

The superconducting ECR has been tested up to a platform voltage of 25 kV. However, due to limitations in the ECR to K500 transport system only beam energies compatible with a platform voltage of 20 kV can be effectively transported to the K500 at the present time.

A new second harmonic central region for the K500 [3] has been designed and fabricated, and commissioning is well underway. Existing internal beam probes have been refurbished and bunch length diagnostics have been designed and implemented. The K500 extraction system geometry has been modified appropriately for K500 operation in the K500⊗K1200 mode, although the power handling capacity remains to be developed. Recent results of the ECR through K500 extraction system are given in Table 4. These initial results are quite encouraging since the K500⊗K1200 specifications are nearly met even though

Item	Achieved	K500⊗K1200 Specification
ECR to K500 Transmision	≥50%	50 %
ECR Voltage	20 kV	≤30 kV
K500 Injection Efficiency	~5%	6 %
K500 Extraction Efficiency	~80%	90%
Overall Transmission	~2%	2.7%
Extracted Emittance (πmm-mrad)	~10	~3

Table 4: Results achieved to date compared to K500 specifications for the K500⊗K1200 system.

critical elements such as the improved ECR to K500 injection line remain to be implemented. Bunch lengths meeting design specifications (3° FWHM) and intensities at ~ 55% of the design requirement (6×10^{12} particles/s) have been achieved, although not simultaneously. In the near term, efforts will be directed towards achieving the nearly realized goal of extracting beams from the K500 which meet the K500⊗K1200 specifications.

References

1. Richard C. York, T.A. Antaya, Henry Blosser, Don Lawton, Felix Marti, D.J. Morrissey, B.M. Sherrill, John Vincent, and A.F. Zeller, "Present Status and Future Possibilities at NSCL-MSU", Proc. 4th European Part. Accel. Conf., London, England,June 1994,pp. 554-556.
2. "The K500⊗K1200 - A Coupled Cyclotron Facility at the National Superconducting Cyclotron Laboratory", July 1994, Michigan State University, East Lansing Michigan, MSUCL-939.
3. S. L. Synder and F. Marti, "Study and Redesign of the NSCL K500 Central Region", these proceedings.

STUDY AND REDESIGN OF THE NSCL K500 CENTRAL REGION

S. L. Snyder and F. Marti

The proposed K500-K1200 cyclotron coupling project calls for a redesign of both the inflector and central region of the K500. An increased injection voltage will be needed to reduce space charge effects in the higher intensity beam. In order to obtain stripping injection matching with the K1200, the K500 will operate in the second harmonic rf mode. To meet the requirements of this higher energy beam (and new rf mode) a new spiral inflector and central region geometry are needed.

1. System Design

An increase in the axial height (for ease in construction) and gap size (for improved acceptance) over the present inflector was studied and comparisons of the two inflectors made. Acceptances in initially uncoupled x,v_x and y,v_y phase spaces were calculated as were the effects of changing the axial field by way of a solenoid along the injection route. An inflector field of 20kV/cm was chosen to maximize the final radius in a 4.6 Tesla central field. This results in a 1.96 cm final (inflector exit) central ray radius and an inflector height of 3.00 cm.

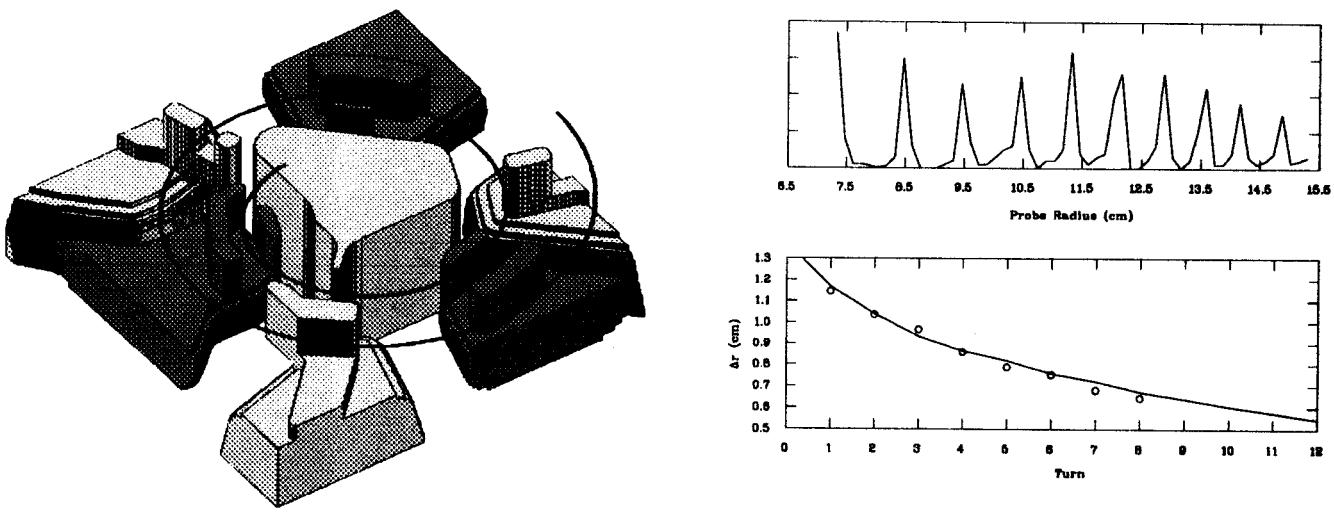

Figure 1: Left: The 2^{nd} harmonic central region design. Shown is a cutaway of the central region electrodes below the magnetic median plane. Right top: Differential probe trace in the K500. Right bottom: Δr vs. turn for the same. Circles represent data while the curve was calculated from orbit tracking.

Once an inflector shape was determined a second harmonic central region was designed. All electrode shapes and positions had to accommodate the new, larger inflector housing and guide the beam through the central region leaving it reasonably well centered. The dee voltage chosen for the O^{+3} test case was 70kV (well below the 80kV which can be reliably achieved) with a chosen minimum electrode separation of 8mm. With these considerations in mind a central region was designed that produced a well centered beam with good vertical focusing properties. Figure 1 shows the central region so obtained as well as the path of the central ray. The figure was used as input RELAX3D run with grid dimensions $\Delta x=\Delta y=.0254$cm and $\Delta z=.127$cm. The vertical grid is clearly visible as steps in the hill shape. This figure

also shows the first turn phase selection slit (located at θ=110°) which will be used to limit the phase width of the beam.

2. System Acceptance and Phase Selection

In order to determine the acceptance of the new 2^{nd} harmonic central region and inflector system, a set of ions were tracked from 3.0m below the median plane of the K500, up the magnet axis, through a 1^{st}+2^{nd} harmonic buncher, the spiral inflector and out through the K500 central region. The critical value determining the effectiveness of the design is the percentage of the input DC beam which maps into the final 3° bandwidth required by the K500-K1200 coupling project. To calculate this, a range of emittances were tracked up the machine axis and through the spiral inflector. Each set of starting conditions consisted of a uniform circular distribution of points (one point per mm-mrad) spanning the coupled emittance area in x,p_x and y,p_y. To simulate the time structure of the incoming beam a series of coupled $x,p_x/y,p_y$ sets were started each separated by 2° RF. This now complete set of starting conditions was then passed through the K500 axis elements (a single solenoid and buncher), through the inflector and out past the K500 phase selection pins.

Presently, the K500 is equipped with two phase pins located on the 0° and 120° hills at a radius of 18cm. These pins consist of two movable tungsten blades that are used to intersect the beam thus limiting its phase width. As mentioned above, there is a third slit, consisting of a fixed aperture window, located on the first turn. Thus there are three apertures which may be used in phase selection.

To model the effect of these slits a program was used which simulates the effect of various slit combinations. The program identifies which ion orbits (if any) intersect with each pin and removes these from consideration. The final collection of surviving ions is then binned according to final phase and a beam timing spectra is produced. Additionally, a variable width, first turn, window slit can be inserted to further reduce the final timing spectra. By using the r,ϕ output of the central region orbit code a measure of the acceptance of the cyclotron into a 3° FWHM timing region which can be expressed as a percentage of the input DC beam (at z=-3.0m) surviving for various starting emittances and buncher modes. For an initially 75π mm-mrad phase space 6% of the DC beam is placed in the final 3° FWHM timing spectra.

3. Experimental Results

The new K500 central region and inflector have been built and are currently being commissioned. As a check on the reliability of the orbit code calculations measurements of radius gain per turn were made on the O^{+4} beam. Figure 1 shows a differential probe trace and a comparison of measured values with those obtained from computer runs. By varying starting time of the calculated central ray good agreement between the two can be reached. Measurements of the internal bunch length have been made using both the first turn slit and phase selection pins. A 3° FWHM bunch length has been observed for the internal beam.

4. Conclusions

A new inflector and 2^{nd} harmonic central region have been designed to meet the specification of the K500-K1200 coupling project. Beam orbit calculations show that a 3° FWHM bunch length, with good transmission properties can be achieved. The new design has been installed and early results support the design's calculated properties.

BEAM TIMING PROBE DEVELOPMENT FOR COUPLED CYCLOTRON

J. Yurkon, F. Marti, T. Grimm, R. Ronningen, and J. Ottarson

In order to position the Phase Slits of the K500 cyclotron it is necessary to have a beam probe to measure the time structure of the primary internal beam.

We looked at three different probes. One of the probes, based on a Silicon Avalanche Photo Diode (APD), was reported on earlier[1]. The APD Probe detects photons produced when the beam strikes and stops in a metal target on the probe. Protecting the APD from the primary beam in this manner yields a long lifetime for the probe because the electrons produced by the x-rays are much less damaging than the heavy ion beams. This probe has been successfully used, and a typical spectrum is shown in Fig. 2. APD's give very good timing because of their fast rise time. However, due to the large range of pulse heights it is necessary to carefully optimize the walk ajustment of the constant fraction discriminator. Also, there may be delayed signals from charged particles or secondary electrons from the metal target.

Detectors which rely on detecting the primary beam do not need nearly as much care because the straggling of the primary beam is relatively small compared to the large range of energies deposited by secondary x-rays. A very simple detector based on a PIN Photo Diode from Micron Semiconductor was tried. It provides very good timing and is easy to setup because timing walk is no longer a problem. However, the primary beam must be carefully attenuated in order to protect the PIN Diode from radiation damage. A typical spectrum is shown in Fig. 2. The construction of the probe is shown in Fig. 1.

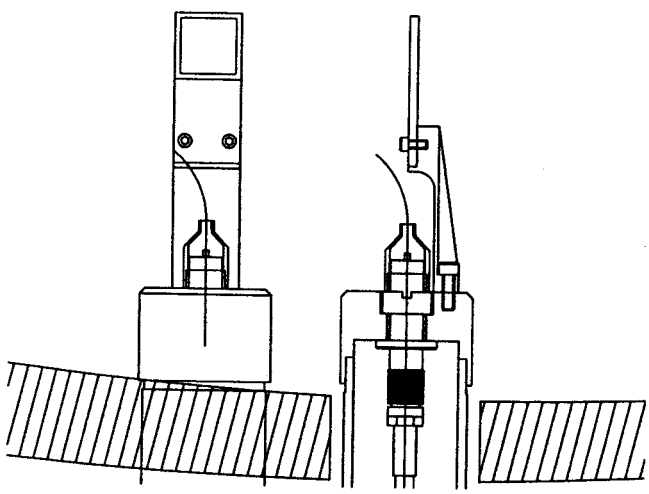

Figure 1: PIN Diode Beam Timing Probe.

Scintillators are less easily damaged so we attempted to design a probe based on a plastic scintillator (Fig. 3). A 1 square centimeter, 2 mm thick plastic scintillator was coupled to a plastic fiber light guide in order to keep the PMT away from the strong, stray magnetic field of the cyclotron. A 1mm diameter fiber would collect less than 5% of the light. By using a wavelength shifting fiber it was thought that we could improve that to between 10% to 20% collection efficiency. This was not successful, at least

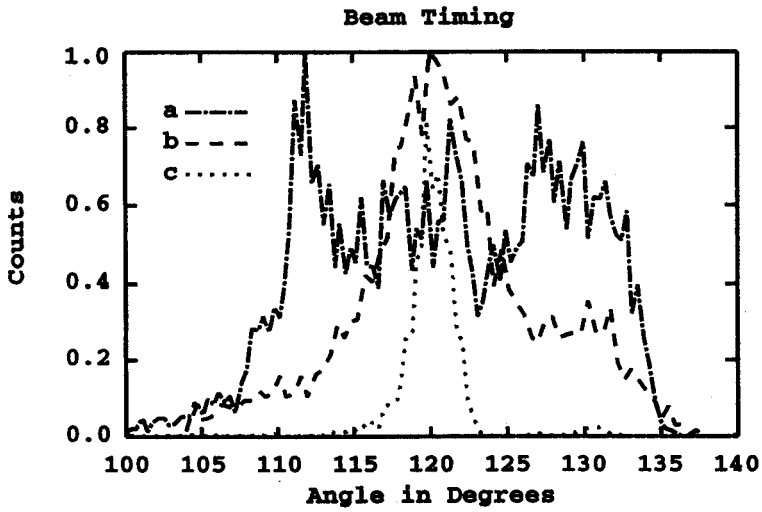

Figure 2: Beam Timing. a) = Bare PIN Diode, b)=APD and first turn slit, c)= Bare PIN Diode and Phase Pins.

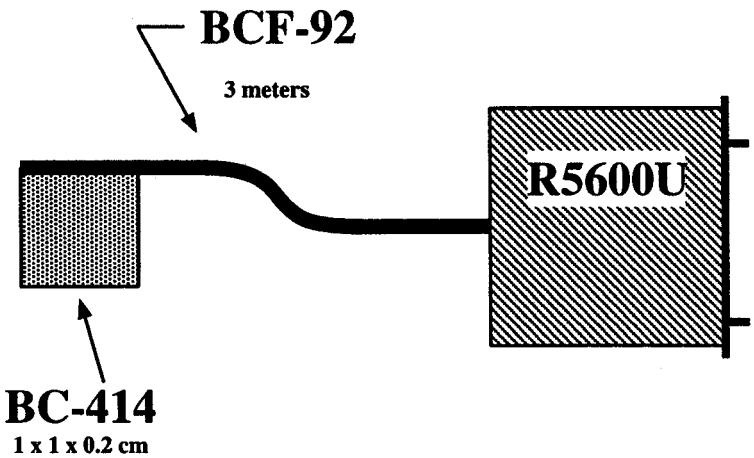

Figure 3: PMT Scintillator Beam Timing Probe.

for 16 MeV/u ^{16}O, because of the slow response of the wavelength shifter (6 nsecs) coupled with a smaller than expected light collection efficiency.

We found the R5600U PMT, from Hamamatsu, to be nearly immune to the fringe field of the K500. So, we are planning on testing an improved design using a 1cm diameter light guide coupled directly to the PMT. This should yield greatly improved light collection and thus improve the timing.

References

1. R. Ronningen, J. Yurkon, M. Maier, NSCL Annual Report, 126 (1988).

S800 PROGRESS REPORT

A. Zeller, B. Sherrill, S. Alfredson, S. Bricker, J. Caggiano, J. DeKamp, R. Fontus, H. Hilbert, P. Johnson, H. Laumer, A. McGilvra, L. Morris, D. Pendell, D. Sanderson, R. Swanson, R. Welton, and B. Zhang

This has been a year in which a very large effort has been put into S800 construction, and a number of important milestones have been reached. Notable successes were the operation of the first of the two dipoles and the measurement of its field with the mapping system.

The first of the two dipoles, D1, was installed onto the carriage and connected to the cryogenics. Unfortunately, a small helium leak appeared in the system. Tests indicated the leak is in the bobbin and the only way to fix it would be to completely disassemble the magnet. It was decided instead to install several diffusion pumps to try to keep the pressure at a level low enough to allow operation. Upon cooldown the heat load was found to be barely within the capabilities of the CTI-1400. Over a period of about two weeks the leak appeared to partially plug up and the pressure droped by a factor five. When in this mode, the heat load is ten watts, which is well within the range which will allow operation.

The magnet was successfully operated at the design peak central field of 1.6 T at 436 A. A plot of the measured field versus current is given in Fig.1. The magnet did not quench nor show any signs of instability. The field mapper was then installed and debugging started. Preliminary maps (the final maps have to be done with both dipoles in place) will be taken early in 1995.

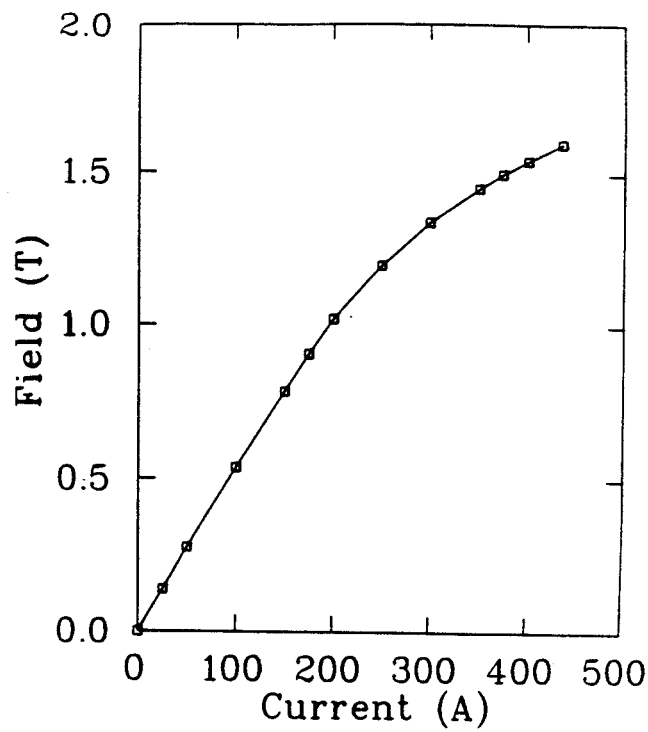

Figure 1. The measured magnetic field of the first dipole, D1, as a function of current. The nominal operating field for k=800 is 1.5 T.

Preparation of the bobbin for D2 was done and coil winding started. The leak checking of the D2 coils can be seen in Fig.2. In this photo one can also see the top of the completed D1. Winding was

completed and preparation for sealing the coils in the bobbin was started and will be completed early next year. Installation of the trim coils and cryostat work was started.

Installation of the platforms on and around the carriage was started. The shielding support in the beamline has been installed. Work on the vault utilities is underway.

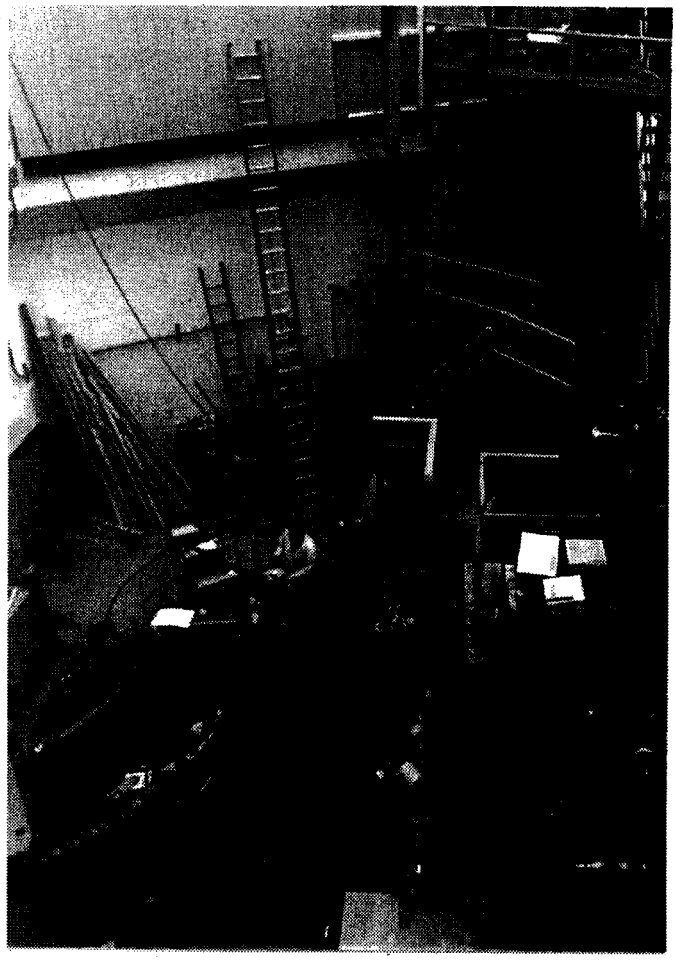

Figure 2. A view into the spectrograph pit at the end of 1994. The main coils for D2 are being leak checked. On the right side of the photo are the elevator and permanent platform. At the bottom right, the top of D1 is visible.

Reports on the beamline, Q1/Q2 and the detector can be found in other sections of the Annual Report. Completion and installation of all components is scheduled for the end of 1995.

S800 BEAMLINE MAGNETS AND SPECTROGRAPH QUADS PROGRESS

J. DeKamp, S. Alfredson, R. Swanson, J. Wagner, A. Zeller

The first of the superconducting quadrupole triplets[1,2] for the beamline to the S800 spectrograph[3] is 50% complete. Two of the 4 dipole bobbin cryostats are complete as well as all 4 of the dipole upper cryostats which provide cryogen holding capacity for the bobbin cryostats. A LHe bucket for the large dunking dewar is being fabricated which will allow testing of 3 quadrupole magnets at once before assembly into their cryostats. The steel assemblies are in house for the spectrograph quadrupoles Q1 and Q2, and test winding of their potted coils is in progress. The He leak in the quad doublet to be used at the beginning of the beamline has been repaired and the doublet is now installed. Design of a field mapping device which accommadates both the triplets and the Q1/Q2 doublet is in progress.

S800 Beamline Quadrupoles

Coil winding and magnet steel machining for the 18 assemblies (enough for 6 triplets which includes a spare) was completed in July, 1994. Precision spacer bars were also machined which connect 3 steel assemblies into a triplet. A 4 ft. by 6 ft granite surface plate was purchased to provide a precision surface for aligning the steel assemblies as a triplet to within 0.005". The first triplet magnet assembly was completed in August and is shown in Figure 1. The magnet assembly was then rotated to the verticle position, being supported by one vessel head and the bore tube of the LHe container. The LHe vessel cylinder and other head were then installed and welded along with necessary wiring being done for connection later to the vapor cooled current leads as shown in Figure 2. The assembly was then rotated back to the horizontal position where the LHe container reservoir, current leads, feedlines, and safety vent pipe were welded completing the LHe vessel assembly. The LHe vessel/magnet assembly was then again rotated to the verticle position for installation of the LN_2 container/shield tube assembly after which it was rotated back horizontal again for the remainder of the cryostat assembly. The LHe vessel surounded by part of the LN_2 cooled thermal shied is shown in Figure 3. Completion of the triplet cryostat including insulation, support link assembly, and cryostat wall assembly should occur in March, 1995. All necessary parts are now in house. Enough magnets have been assembled for the second triplet and it's LN_2 container/shield tube assembly is also done. A bucket for the large dunking dewar is being constructed to hold the 3 magnets for testing before assembling into a triplet. This was felt to be necessary since we did not have a fully successful prototype magnet test until our 3rd set of coils.

S800 Beamline Dipoles

Two S800 beamline dipole bobbin cryostats are complete with 1 cryostat welded to it's poletip assembly as shown in Figure 4. These dipoles are similar to ones previously built[4] except for their orientation to bend the beam vertically and their larger gap (7cm vs. 5cm). All 4 upper cryostat assemblies are now complete. The upper cryostat assemblies are later connected to the bobbin cryostats after assembly to the yoke steel.

S800 Spectrograph Q1/Q2 Quadrupole Doublet

Design of the spectrograph doublet, Q1/Q2, is in progress and some of the parts are now in-house. The design is complicated by it's close proximity to the first spectrograh dipole downstream and a scattering chamber to be upstream. There is also a superconducting sextupole mounted within the Q2 magnet, mounted to the LHe vessel bore. Support links and hardware; some cryostat, LHe vessel, and LN_2 cooled shield parts; and both machined steel assemblies have arrived. The Q1 and Q2 steel

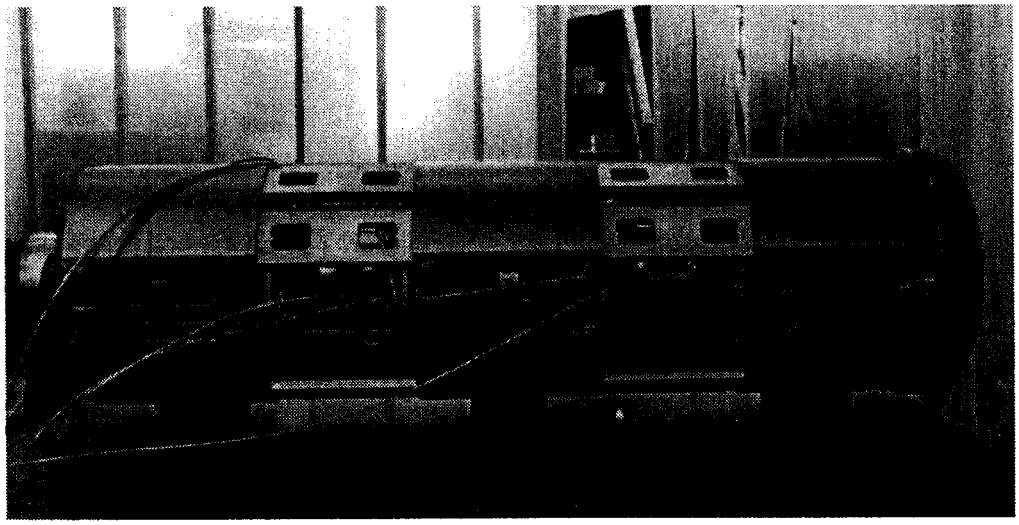

Figure 1: S800 beamline quadrupole triplet magnet assembly after alignment on granite surface plate.

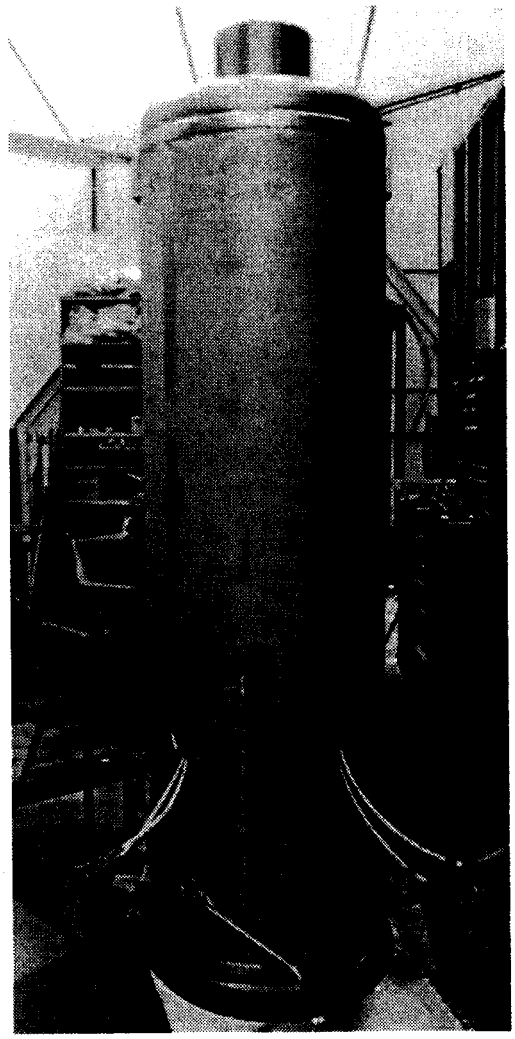

Figure 2: Quad triplet LHe vessel cylinder containing triplet magnet assembly. The LHe fill line and current and instrumentation leads protrude from the vessel for later connection within vessel hat.

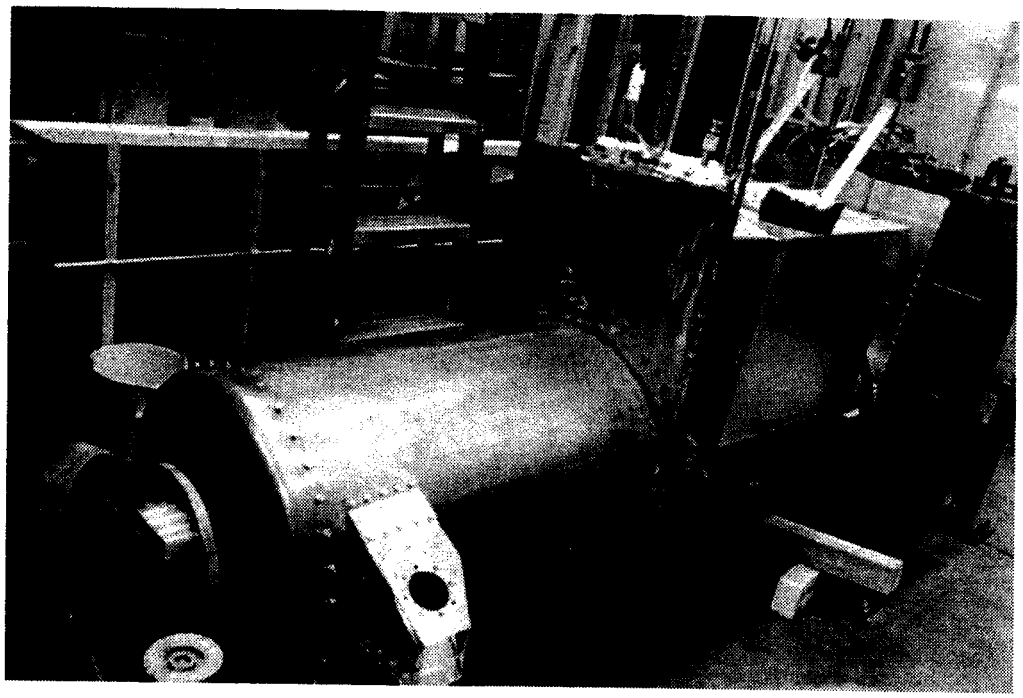

Figure 3: Quad triplet with LHe vessel completed and shield partially assembled.

Figure 4: Dipole bobbin cryostat assembly welded around poletip assembly to maintain beam vacuum.

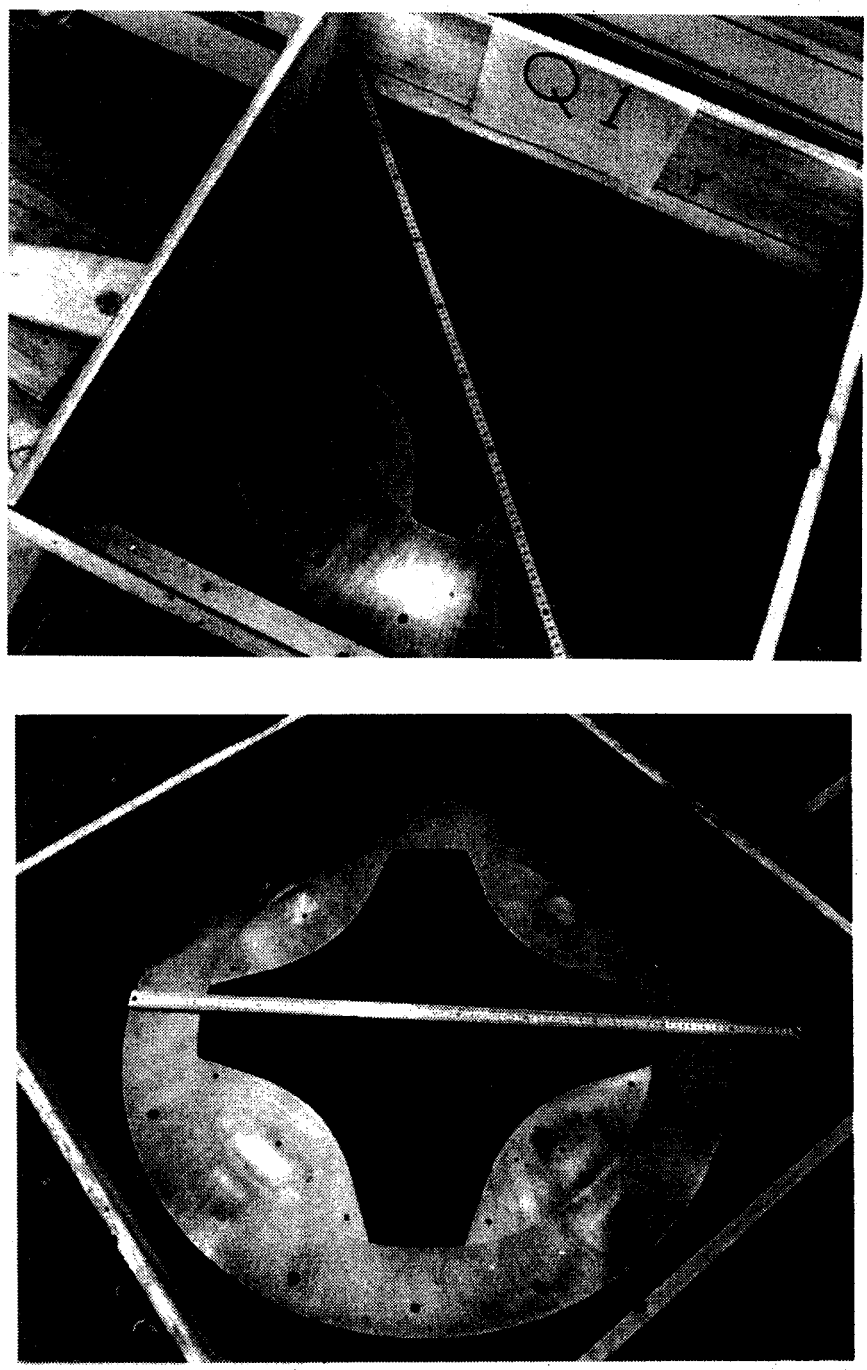

Figure 5: Q1 and Q2 quadrupoles steel assemblies. A meter stick is placed across the ends for size reference.

assemblies are shown in Figure 5. The conductor spools have arrived and all winding forms are complete. Test winding of the coils for Q2 is in progress.

References

1. J.C. DeKamp et al., "Superconducting Beamline Quadrupoles and Dipoles Progress", MSU Annual Report (1993), p. 196.
2. A.F. Zeller et al., "Superconducting Beamline Elements for the NSCL Spectrograph", IEEE Trans. on Applied Superconductivity, (in press).
3. A.F. Zeller et al., "Construction of a Superconducting Spectrometer Dipole Magnet", Advances in Cryogenic Engineering 37, Part A, 417(1992).
4. J.C. DeKamp et al., "Superconducting Beamline Magnet Progress", MSU Annual Report (1988), p. 157.

FURTHER TESTS OF THE EIGHT TESLA MAGNET

Jeff Schubert, Henry Blosser, and Guenter Stork

Commissioning of the Eight Tesla Magnet continued during 1994, with the goal of readying the magnet to be a reliable component in an ultra high field cyclotron [1]. The magnet's liquid helium consumption was studied in greater detail, as were the causes of unexpected quenches.

Heat Load Measurements

The total heat load on the cryostat was calculated as the sum of conduction through the current leads (1.0 l/hr, or 1.4 W at 0 amps), radiation through the nitrogen shield and superinsulation (0.04 W), and conduction through 9 support links (0.15 W), for a total of 1.6 W [2]. Heat conduction through the He gas in the rupture-tube should be negligible.

Several boiloff curves were recorded to infer a lower limit for the steady state heat load of the cryostat, and also to determine the location of excess heat leaks. A typical boiloff curve is shown in figure 1. For a constant pressure, the slope of the boiloff curve is directly proportional to the heat load in watts and the volume of the helium can. The cross section of the can increases at the median plane bridge, so the slope of the boiloff curve decreases even though the rate in liters/hour may be constant.

The slope of the boiloff curve as a function of liquid level has been calculated and converted to heatload in figure 2. The change in cross section at the median plane has been factored out of this calculation. However, small changes at the top and bottom of the median plane appear as "notches" in the heatload curve. The power dissipated by the helium level sensor (ranging from 0 W at 100% to 1 W at 0%) has been subtracted, although part of this power would be carried away by the exiting helium gas and should not effect the boiloff rate. If the entire heatload of the sensor is removed, then the heatload at the bottom of the cryostat is within error of the calculated rate of 1.6 watts.

Moving down the cryostat, abrupt drops in the heatload curve indicate that a source of heat is removed from direct contact with the liquid as the liquid level drops past that level. Therefor we can see that small excess heat leaks are localized at the median plane and at the separations between small and large coils.

The dominant heat leak, at the top, is unfortunately the least reproducible. In four other boiloffs, the peak apparent heatload varied from 10 to 13 W. The true heat load is obscured by effects of falling pressure (flashing) after the fill valve is closed, and possible introduction into the cryostat of warm gas from transfer line. For these reasons the first 15 minutes of a boiloff curve are usually disregarded [3]. Therefor the high heatload region spanning the entire upper small coil is unreliable, and we can only infer a lower limit of 6 watts for the full cryostat. Any heatload beyond 6 W is assumed to be coming from the top of the cryostat.

The steady state heat load was also measured by filling the cryostat continuously from the 500 l dewar, which was itself being filled by the cti1400 refrigerator. The rate of liquid buildup in the dewar with the cryostat connected was then subtracted from the rate of buildup without the cryostat, yielding a difference of 11.3 l/hr. This translates to a 29 W load for the entire system connected to the reliqiufier [4]. The heatload of the 500 l dewar is small, but the transfer lines have an estimated minimum heat load of 3.0 W, which would indicate a 26 W heatload in the cryostat. Although this is at least double the boiloff heatload estimate, only one operational estimate has been made so far. Variances for this type of

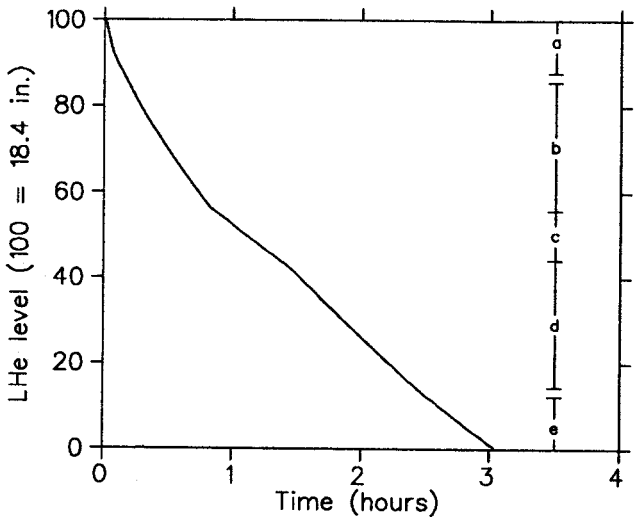

Figure 1: A typical boiloff curve for the cryostat. The slope is initially as high as 25 l/hr, but quickly settles to values below 10 l/hr. The slope near the bottom is roughly 3 l/hr. Lettered scale indicates the magnet geometry. a: upper small coil. b: upper large coil. c: median plane bridge. d: lower large coil. e: lower small coil. Note that the small coils extend .39 in. beyond the top and bottom of the sensor.

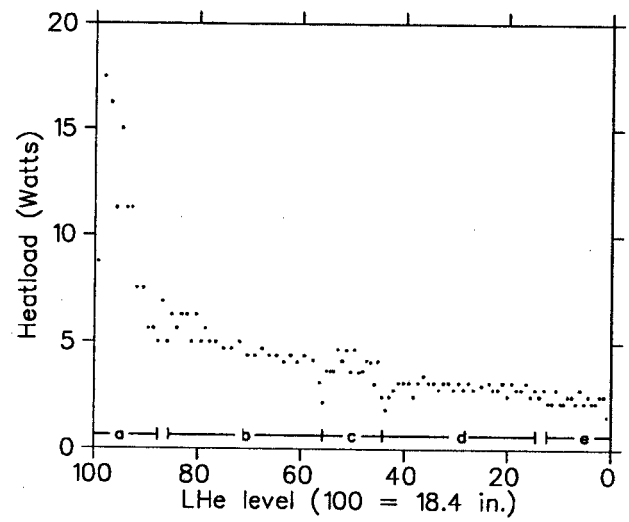

Figure 2: Heat leak as a function of LHe level. The large apparent heat leak near the top of the cryostat may be due, in part, to non equilibrium conditions that occur after shutting off the liquid helium transfer. Dips above and below the median plane bridge are artifacts of the cryostat geometry. Lettered scale is same as in figure 2.

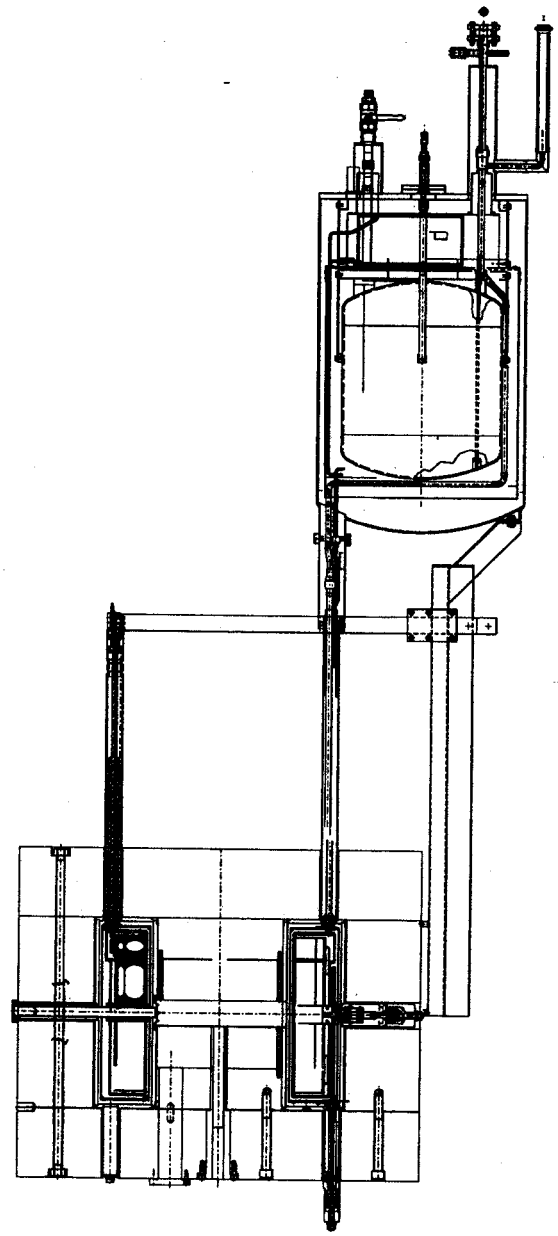

Figure 3: Schematic of coil cryostat with 150 l reservoir. The reservoir would enable the magnet coils to be fully covered at all times, with Helium vapor pressures as low as approximately 1 psig, the minimum required to push cold gas through the current leads.

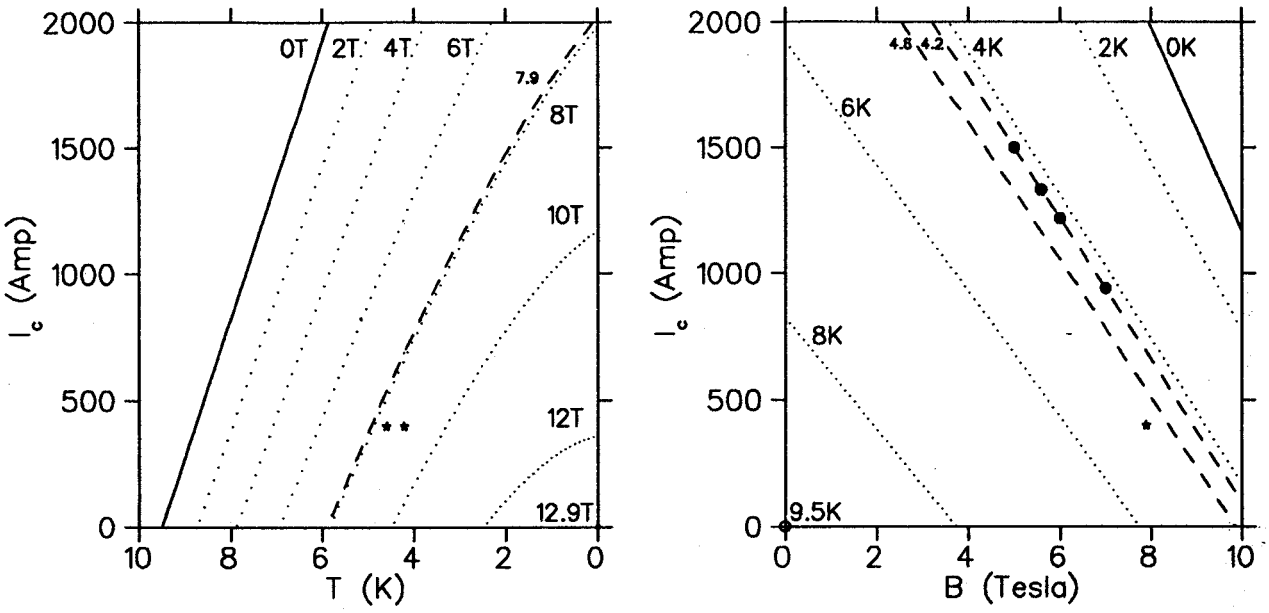

Figure 4: Two views of the approximate critical-current surface for Nb-46.5Ti. The volume below the surface in T-B-I space is in the superconducting phase. Left: Contours of critical current as a function of temperature, for several values of magnetic field perpendicular to the wire. Right: contours of critical current as a function of field, for several temperatures. Peak transverse field in the magnet coils is 7.9 T at 400 amps, denoted by a star on the right, and two stars on the left, one T =4.22 K (atmospheric pressure) and the other for T =4.6 K (helium vapor at 6 psig.) ($I_c(B,T)$ is extrapolated from the manufacturer's short sample test results at 4.22 K (dark circles) and literature values for T_c of similar alloys (light circle.) The approximate relations used are valid for regions of the graph near the data and far from the corners at B_0 =12.9 T and I_0 =5200 A.)

measurement are typically on the order of 10-60% [4].

In the future we plan to install a 150 liter reservoir above the magnet cryostat (figure 3), so that the magnet can operate in batch fill mode. Liquid in the reservoir will then be able to reach an equilibrium pressure and boil off for hours while the coil cryostat itself is completely full, allowing a much more accurate measurement of helium consumption under operational conditions.

Possible Causes of Quenches

The peak field achieved so far with the magnet is 8.2 T with the large and small coils energized to 420 A and 370 A respectively. Although the large coil set, operated alone, has reached 470 A, the design current combination of 400/400 A has not yet been reached. The preponderance of evidence suggests that most or all quenches originate in the small coil set. However, the exact cause of quenching has not yet been determined [5].

The discovery that recent experiments, and possibly all previous experiments, had been conducted at a temperature of 4.6 K, rather than 4.4 K as thought, reopened the question of whether the superconducting wire had exceeded its short sample critical current. The critical current "surface," plotted in figure 4, is a function of both temperature and magnetic field perpendicular to the direction of current flow. The critical current is the maximum amount of current that the NbTi can carry in a superconducting state. Any additional current, above the critical current, will behave as if the NbTi were normal. The extra current will produce a voltage drop and will generate heat. In a potted coil, the copper stabilizer and helium bath cannot carry away the additional heat, so the higher temperature will lower the critical current further, resulting in a thermal runaway, and quench.

The current margin m is defined as $m = (I_c - I_{op})/I_c$, where I_{op} is the operating current and I_c

is the critical current for the operating background field and temperature. With 400 A in both coils, and a central field of 8.1 T, the peak field in the coil wire would be 7.9 T. At 4.4 K the current margin would be 35%. Increasing the temperature to 4.6 K reduces the current margin to 26%. (The critical current is lowered from 616 A to 537 A.) The 7.9 T field only occurs at the lower, inside corner of the large coil. When tested alone, the large coil set did not quench until reaching at least 81% of its critical current [5]. If earlier temperature measurements were incorrect,however, then it is more likely that the large coil quenched at 92% of its critical current (I_c = 510 A at 4.6 K with 8.0 T on the conductor.)

The large coil set has been ramped to 440 Amps at 4.6 K (86% of I_c) twice without quenching, further indicating that a current margin of 26% is more than adequate. The peak field in the small coil is only 7.1 T with 400 amps in both coils. Taken alone, the small coils' safety margin is 47% at 4.6 K. If the quenches do, in fact, originate in the small coil set, then we may rule out the possibility of exceeding the short sample critical current.

Usually the only other cause of quenching is wire movement. However, a third possible factor has been discovered: The active part of the liquid helium level sensors does not reach all the way to the top of the small coil. While the cryostat allows the magnet to be fully covered with liquid, as much as .39 in. (or 14%) of the upper small coil might be above the liquid bath while the sensor reads 100%. The thermal conductivity of 4 K Helium gas is roughly 30% that of liquid [6]. While this is sufficient for some potted coils, The magnet has quenched 3 times with currents of less than 250/250 A, and all three occurances were linked to the liquid level suddenly dropping to 92-99% (exposing as little as .7 in. of the small coil before quenching.) At higher currents, a smaller level drop may sufficient to render the small coil unstable. Similar events may have occured where the liquid level never had time to drop below 100%. Insufficient cooling may act to exacerbate the effects of a loose wire segment near the top of the small coil, or it may simply allow part of the coil warm to a point where it's current margin drops to 0%.

Improving Magnet Performance

The need to cover the superconducting coils completely is the primary motivation for plans to install a reservoir above the cryostat (figure 3). In between fills, the reservoir will also have the additional advantage of allowing the magnet to operate at pressures as low as 1 psig, thereby lowering the temperature of the helium bath from 4.6 to 4.25 K, and raising the critical current at 7.9 T from 537 A to 675 A. While the additional safety margin is, in principal, unnecessary, it will allow for a wider range of small disturbances, such as small wire movements, that might have otherwise generated sufficient heat to cause a quench.

References

1. J. Schubert, Initial design studies for an ultra high field K80 cyclotron, this Ann. Report.
2. J. Kim, Ph.D. Thesis, MSU (1994).
3. H. Laumer and M.L.Mallory, MSU-CL Ann. Report, 244 (1984).
4. H. Laumer, NSCL Ann. Report, 176 (1992).
5. J. Kim, NSCL Ann. Report, 171 (1993).
6. J. Jensen et. al. Bubble Chamber Group.

INITIAL DESIGN STUDIES FOR AN ULTRA HIGH FIELD K80 CYCLOTRON

Jeff Schubert and Henry Blosser

We have begun serious design studies toward utilizing the Eight Tesla Magnet [1] as a component of an ultra high field cyclotron. Such a cyclotron would use the highest magnetic field, to date. The K80 "Eight Tesla Cyclotron" would have roughly the same magnetic rigidity ($B\rho$) as the Harper Medical Cyclotron in a package only two thirds the size, with corresponding reductions in cost.

This cyclotron could accelerate particles with a charge state, $Q/A = \frac{1}{4}$ to a final energy of between 5 and 6 MeV/nucleon, the energy range currently being used to study superdeformed, high angular momentum nuclei that result from glancing collisions [2]. Our first goal is to develop an internal beam, starting with a simple PIG ion source. Later the cyclotron could be modified to incorporate an external ion source, and to allow for beam extraction, which would be necessary for most nuclear physics experiments.

Studies thus far have stressed achieving sufficient vertical focusing (ν_z) despite the high field level.

General Parameters

For simplicity, we envision a fixed energy, single charge state, machine. The design is optimized to accelerate He^+ ions ($Q/A = .2516$). As in the Harper cyclotron, the field will be shaped by hill and valley shims, so no trim coils will be needed. With a central field of 7.6 T, (see following section) and a final radius of 7 in., the magnet's bending limit is $K_b = 83$ MeV.

Operating in 3rd harmonic at a dee voltage of 33 KV, the RF frequency would be 87.11 MHz, which is near lower limit of available commercial FM transmitters. A beam which crosses each gap when the RF voltage is at its peak would require 106 turns to reach a final energy of 5.24 MeV.

Magnetic Field

The Eight Tesla Magnet has a split coil design similar to the K1200 magnet, with a primary coil set, denoted "α," near the median plane, and a smaller coil set, "β," located away from the median plane. A current combination of $I_\alpha/I_\beta = 400/300$ A was chosen because this is the highest current at which the magnet has operated reliably to date.

The pole tip design and calculated field for this current combination are shown in figures 1 and 2, respectively. Because all of the iron in the pole tips is saturated, raising the overall field level,$< B >$, has little effect on the third harmonic component, B_3. Our third harmonic rises from zero at the center to roughly 0.8 T near the extraction radius, just as the Harper cyclotron's field does. The ratio of $B_3/ < B >$, then, falls in proportion to $< B >$, so the higher the field the smaller the contribution of flutter focusing to ν_z. Although ν_z is sufficient at middle energies, it rises so slowly that the central focusing cone (and electric focusing) for the first few turns will be more important in high field machines than in their low field predecessors.

We have chosen to use an NSCL standard 1.375 in. diameter ion source. Increasing the field of the cyclotron causes all of the particle orbits to shrink. As the radius of the first turn shrinks, but the central hole does not, the dip in the center of the magnetic field, caused by the hole, becomes more serious. We attempted to compensate for the hole with the center plug, but in the end it was necessary to incorporate iron into the ion source itself. Although this complicates the ion source design considerably, it fills in the field hole completely and makes the shaping of the central field cone (for axial focusing of the first few

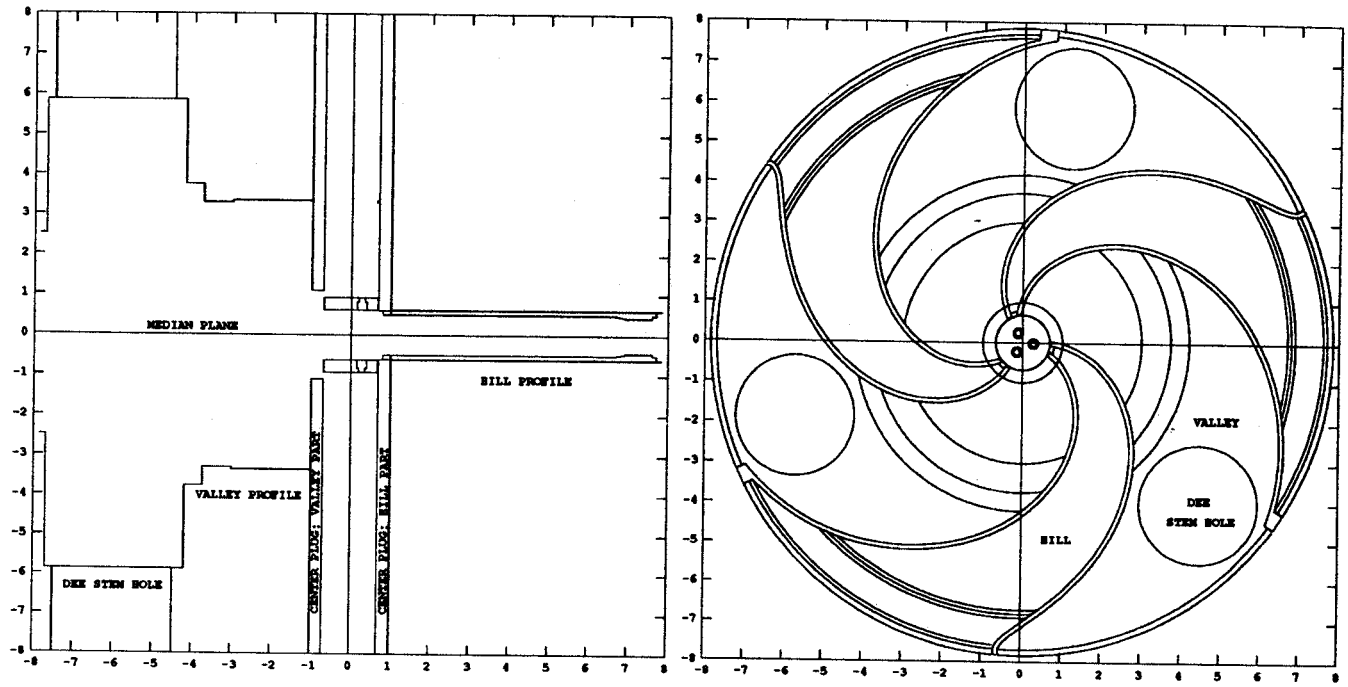

Figure 1: Radial profile (left) and median plane view (right) of pole tip geometry. Chamfers on the hill edges ($r = .25$ in.) and on the inner valley shim ($r = 1.0$ in.) have been approximated by steps which remove the same amount of iron as the actual chamfer. Iron will be incorporated into the ion source (as shown here) or spiral inflector to shape the magnetic field in the central region. Units on the graphs are inches.

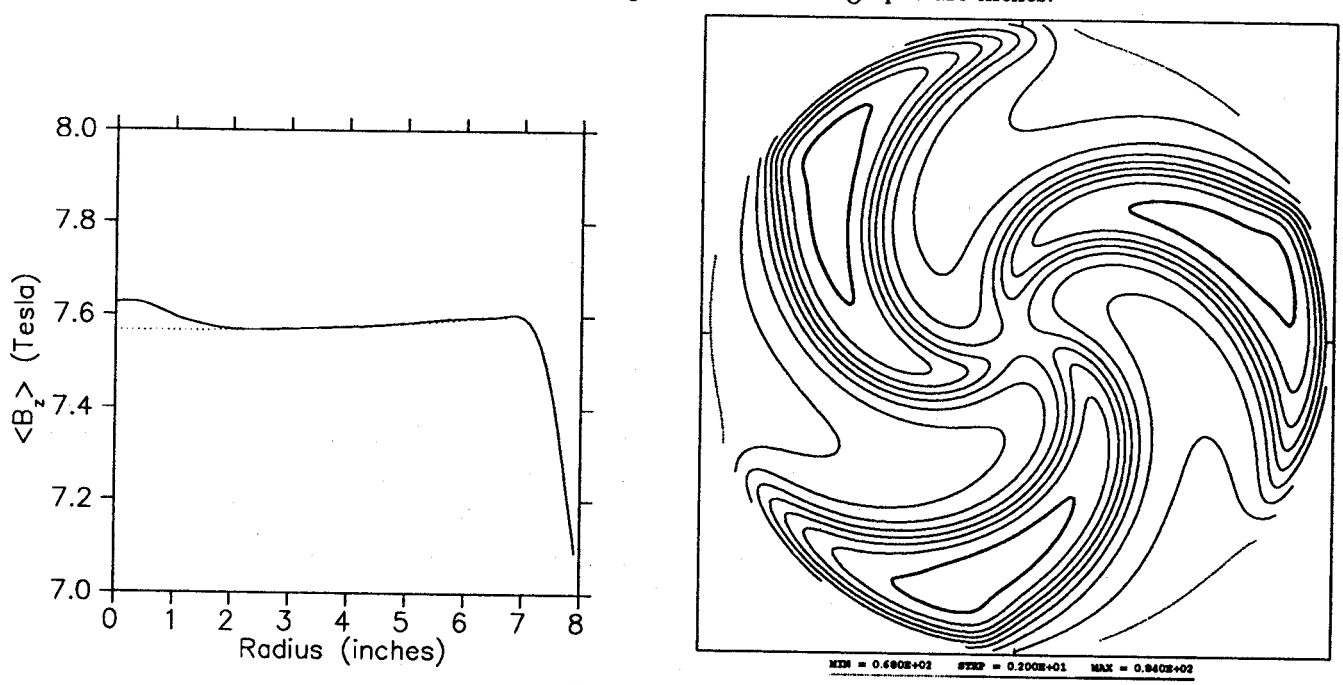

Figure 2: Left: the azimuthal average of the median plane field. Right: contour plot of the median plane field. Contour spacing is two kilogauss with the dotted contour at 6.8 T and the double weight contour over each hill at 8.4 T.

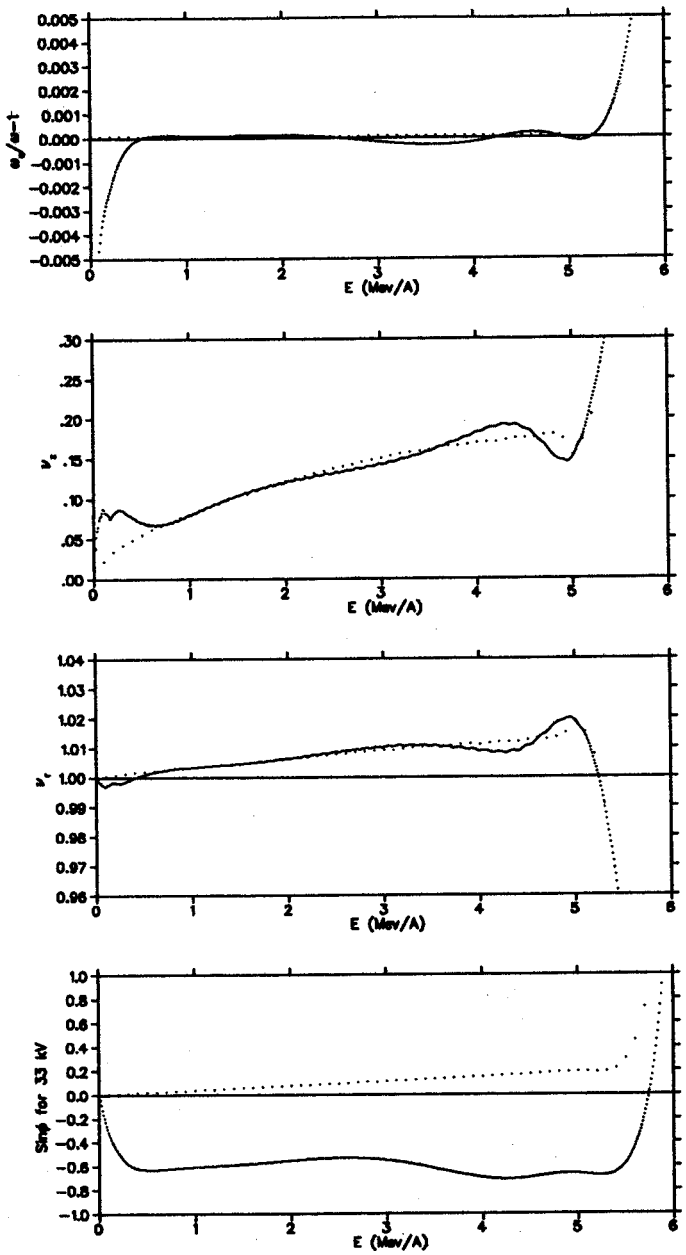

Figure 3: Equilibrium orbit properties as a function of energy. Top: orbital frequency relative to isochronous frequency. Middle: axial and radial focusing frequencies. Bottom: phase. Curves with points spaced at intervals of 0.01 MeV are for the calculated field. Curves with points 0.1 MeV apart are for a field which is perfectly isochronous out to a radius of 6.9 in. The target (or extraction system) would be located near the $\nu_r = 1$ resonance at 5.24 MeV. (The negative offset of the phase curve will be corrected during the design of the central region.)

turns) much easier.

The predicted orbit properties are shown in figures 3 and 4. The large negative offset in the phase plot occurs because our simulation does not yet account for the complicated electrode geometry of the central region. By lengthening the distance from the first acceleration gap to the second, the beam can be forced to arrive later with respect to the RF time (i.e. at a more positive phase) [3]. Thus far we have assumed that the distance from the puller to the second gap will be long enough to increase the phase of the beam to the neighborhood of $sin(\phi) = 0.6$, and the magnetic field was designed to quickly bring the phase back to 0.

The dip in ν_z between 0.5 and 1 MeV could be corrected with a radially larger central cone, however this would also increase the negative phase slip in the first few turns. Only after further central region studies will it be possible to determine whether or not more phase slip is acceptable.

Hardware improvements planned for the near future may make it possible to operate the Eight

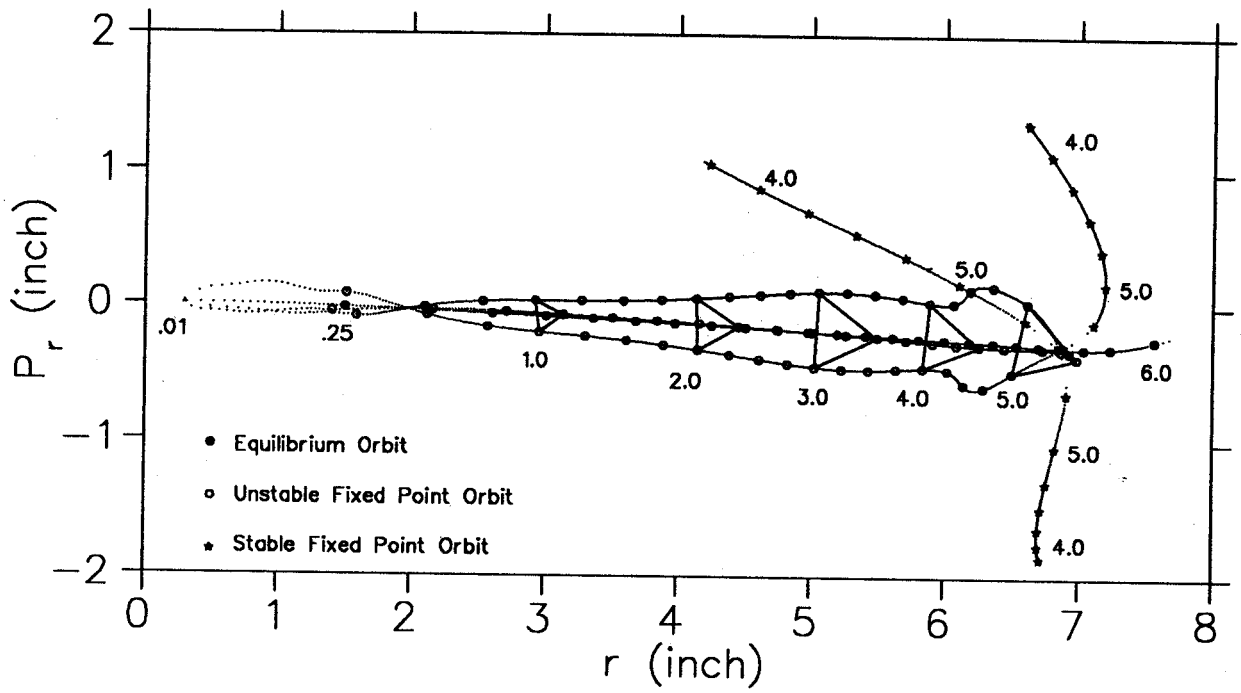

Figure 4: Radial phase space plot of the equilibrium orbit and fixed point orbits. Orbits are plotted once per turn (along a hill edge) yielding a single point for each orbit. Energies are marked in units of MeV. Triangles connecting the three unstable fixed points for a given energy contain the stable phase space area for that energy. Without acceleration, any particle in the stable area would circle the equilibrium orbit, never leaving the triangle.

Tesla Magnet at it's design current of $I_\alpha/I_\beta = 400/400$ A [4]. This would raise the cyclotron's central field to 7.8 T and the final energy to 5.58 MeV. Only minor changes in the pole tip design would be required.

Central Region

Central regions for multiparticle cyclotrons are designed using a reference particle and the Reiser parameter, χ, which dictates dee voltages and/or field levels to guide different particles through the same central region geometry [5].

$$\chi = \frac{l_1^2 B_1^2 (Q/A)_1}{V_1} = \frac{l_2^2 B_2^2 (Q/A)_2}{V_2} = constant,$$

where B is the magnetic field strength at a reference point, Q/A the charge state in units of e/m_0, V the peak dee voltage, and l a reference length, usually the dee gap. The subscript 1 refers to the reference particle and 2 refers to any other particle. The same relationship may be used to expand or reduce the central region from one machine to work for a different particle in a different machine. For two given particles, magnetic fields, and dee voltages, system 2 will be a photographic enlargement of system 1 by a scale of $l_2 : l_1$. The Harper Medical cyclotron accelerates deuterons ($Q/A = \frac{1}{2}$) in a central field of 4.6 T. Using the same dee voltage, and an internal PIG ion source, we need only reduce the dimension of Harper's central region by a factor of 0.86 for the Eight Tesla Cyclotron. Minor changes will, of course be required because the radial profiles of the two magnetic fields are not identical. Additional features may also be changed to adjust the initial phase slip of the beam.

Feasibility of Axial Injection

Using the cyclotron as part of a nuclear physics program would doubtless require the capability of axial injection. A spiral inflector design (and new central region) might be scaled from the system used in the K1200 cyclotron by holding the parameter $K = A/2R_m$ constant, where A is the inflector's electric radius of curvature (and the height of the inflector) and R_m is the magnetic radius of curvature in the center of the cyclotron [6]. (The spiral inflector K is not to be confused with K_b of the cyclotron.) The electric field in the inflector gap would then have to increase in proportion to the magnetic field. The K1200 runs He^+ ions in a 3.51 T field. Our field is more than double the K1200's, so we would have to increase the gap electric field from 11 KV/cm to 24 KV/cm, which is still safely below the dielectric strength of a vacuum.

The inflector must, of course, fit within the first turn of the ion orbit. The height and width of the inflector are inversely proportional to the magnetic field, so the dimensions of the inflector will by scaled by a factor of $\frac{B_{K1200}}{B_{8TCyclotron}}$ =0.464. The first turn of the ion orbit scales according to the formula in the previous section. Compared to the K1200, orbits will be reduced by a factor of 0.435. The space between the first turn and the inflector body will be only slightly tighter than in the K1200, so little modification should be necessary to insure that the orbit clears the inflector.

A more serious problem is the overall size of the inflector electrodes. Since the constant-K scaled inflector has a height of just 0.81 cm, and a gap of 2 mm, this design might be too difficult to fabricate. More detailed studies may be needed to investigate the effects of increasing the gap hight (and the corresponding voltage.)

Conclusion

Raising the maximum isochronous cyclotron field from 5 to 8 T is feasible, and axial injection into such a cyclotron is at least conceptually feasible. Further studies of orbit dynamics in the design field are currently underway. Central region and extraction studies will follow.

References

1. J.W. Kim, Ph.D. Thesis, MSU (1994).
2. B. Schwarzschild, Physics Today, Oct. (1991).
3. W.I.B. Smith, NIM. 9, 49 (1960).
4. J. Schubert, Further tests of the Eight Tesla Magnet, this Annual Report.
5. M. Reiser, NIM. 18,19, 370 (1962).
6. J.L Belmont and J.L Pabot, IEEE Trans., NS-13, 191 (1966).

PROGRESS IN FOCAL PLANE DETECTOR DEVELOPEMENT FOR THE S800 SPECTROGRAPH

J. Yurkon, B. Sherrill, D. Morrissey, D. Bazin, J. Brown and D. Swan

In continuing our search for a focal plane detector for the S800 Magnetic Spectrograph[1], we decided to test a Cathode Readout Drift Detector (CRDC) design which has demonstrated excellent resolution at Riken [2].

The CRDC is basically a Single Wire Drift Detector that obtains position information along the wire by induction readout on cathode pads spaced along the wire as shown in Fig. 1. Each pad is read

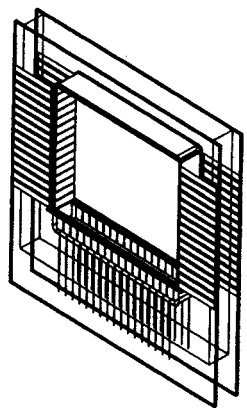

Figure 1: Conceptual View of CRDC.

out individually and the charge distribution is fitted to obtain the centroid. The position along the drift dimension is obtain by simple timing using a stopping scintillator as the start.

We have attempted to investigate the response of the detector to both light and heavy ion beams. We also have varied the pitch of the readout pads and investigated two different schemes for obtaining the charge from the pads. The first is a charge sensitive preamplifier system designed at MSU and the other a TPC readout system developed for STAR [3].

While we are still in the process of this set of tests, we have demonstrated that conventional charge sensitive preamplifiers do achieve, or exceed, the required resolutions of 0.2mm FWHM in Y and 0.4mm in X. Fig. 2 is a histogram of a 60 MeV/u Ar beam irradiating the detector through a mask. A drawing of the mask is overlayed on the Histogram.

Fits to the data yield about 300 μm FWHM in Y and 200 μm FWHM in X. Fig. 3 is a projection of one of the slots overlayed with the fit.

By fitting the charge distribution on the pads to a gaussian, over a limited number of pads it appears that the resolution is improved by ignoring the tails of the distribution which are influenced by delta electrons. Fig. 4 is a typical induced charge distribution measured on the pads. Fig. 5 was produced by finding the center of gravity of the charge distribution. This is equivalent to doing charge division on a wire. Compare the resolution in this spectrum with that of Fig. 2. There is marked improvement over simple center of gravity.

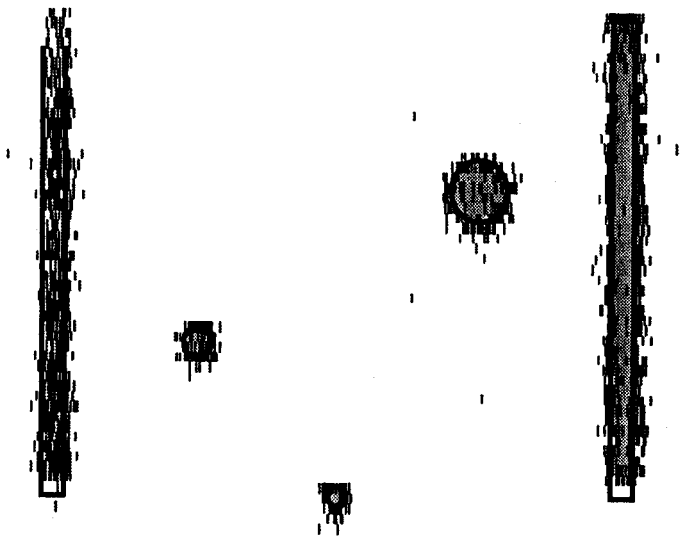

Figure 2: 60 Mev/u Ar Data. The holes are 1,994 μm, 991 μm and 660 μm in diameter. They are separated by 5.0 mm in the x and y. The slots are 813 μm wide and 20.32 mm apart.

The conventional charge preamplifiers were designed and built at NSCL. They are approximately 2 cm by 2.5 cm in size and have a 0.5pf feedback capacitor. They will plug into a motherboard that houses 16 channels. Then 17 of these will inturn plug into the detector.

The STAR electronics would consist of a FEE (Front End Electronics) board, Fig. 6. The FEE board consists of a Preamplifier, Shaper (PASA), Switch Capacitor Array (SCA) and a 12-bit ADC. The SCA samples the signal into 1024 divisions. This provides for Multi-Hit capability since the the charge distribution is measured for the entire drift time of the counter.

We have tested the PASA portion and read it out through a conventional LeCroy FERA. Typical signals are shown in Fig. 7.

When the production FEE boards are available we will begin testing the multihit capability of the

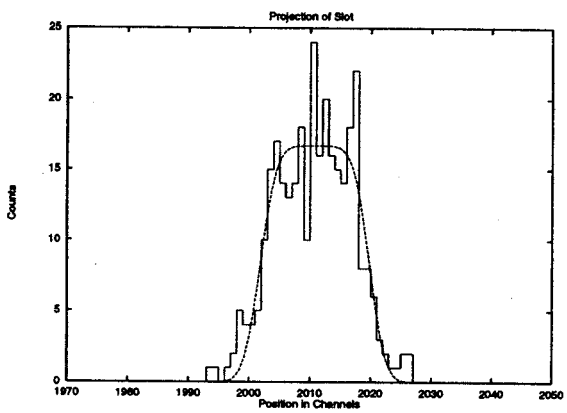

Figure 3: Projection of Mask Slot with Fit.

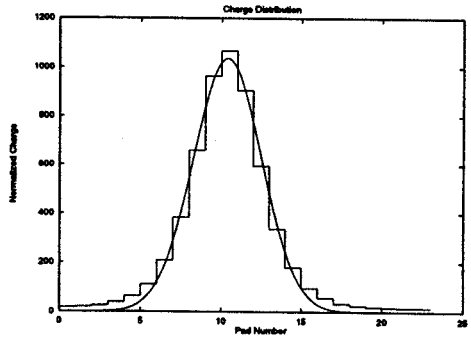

Figure 4: Cathode Pad Charge Distribution.

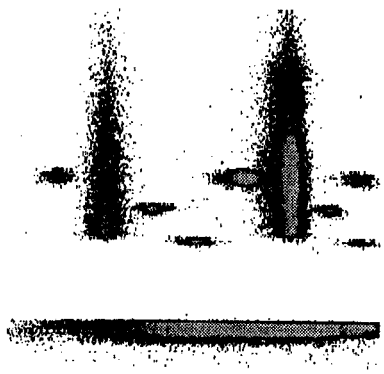

Figure 5: 60 Mev/u Ar Data.

counter and try to determine the real dynamic range. The signal to noise ratio of the production PASA chips are expected to have a four fold increase in dynamic range over the prototypes.

The windows of the counter present a special problem since they must withstand atmospheric pressure over a large area, be fairly thin and yet not have support wires. One design has been tested with used Kevlar 968 Fibre of 195 denier wound onto a 4 inch radius drum covered with Mylar. This is then coated with epoxy and then the resulting windows glued into the pressure window frame which has a cylindrical cut in it to provide the proper radius of curvature for the kevlar as shown in Fig. 8. The material produced so far has thickness of 0.003" and has been tested to 5 atm. The final detector will have a larger window and so the radius will be scaled appropriately producing a window that is expected to hold 3 atm. The prototype was predicted to hold 10 atm but has not been tested at that pressure.

References

1. J. Yurkon, D. Swan, B. Sherrill,D. Morrissey, and M. Steiner, NSCL Annual Report, 200 (1993).
2. Y. Fuchi, M.H. Tanaka, S. Kubono, H. Kawashima and S. Takau, IEEE NSS 92CH3232-6 172 (1992).
3. The STAR Collaboration, LBL Pub-5347 (1992).

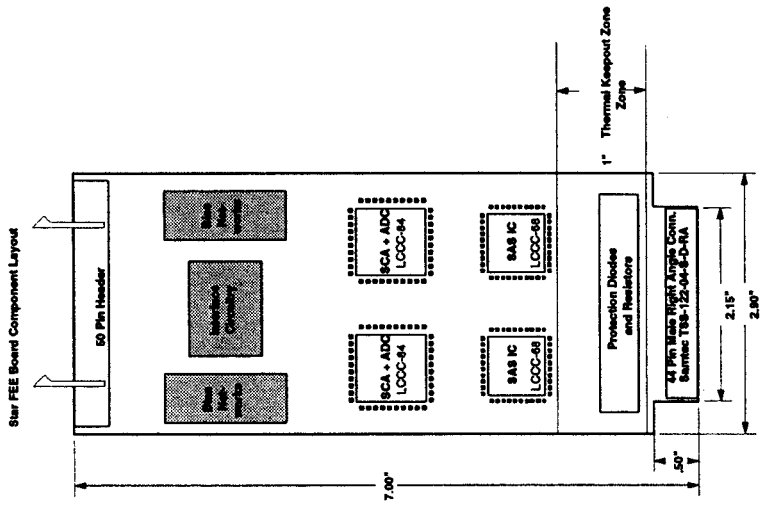

Figure 6: FEE PC Board for STAR.

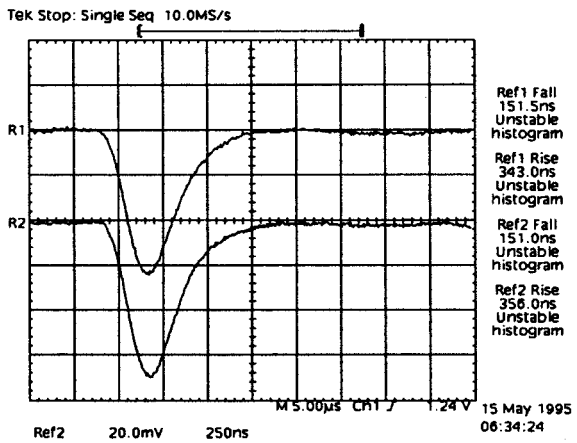

Figure 7: Cathode Pad Signals from FEE.

Figure 8: S800 Pressure Window.

A ZERO DEGREE DETECTOR FOR THE 4π ARRAY

N. T. B. Stone, G. D. Westfall, E. E. Gualtieri, S. Hannuschke, R. Pak,
A. M. Vander Molen, J. Yee, W. J. Llope [a], D. Swan, R. Lacey[b], J. Lauret[b]

We have designed and built a near-Zero Degree Detector (ZDD) and used it in conjunction with the MSU 4π Array. This detector was designed and built in order to identify very forward fragments following the breakup of excited nuclei [1]. Analysis of the data recorded by this detector, still in its preliminary phase, is expected to reveal a monotonic relation between the size of fragments in this detector and the impact parameter of the initial nuclear collision. The detector is shown in Fig. 1. In this drawing, one can identify the eight-fold segmentation of the detector, as well as the independent photomultiplier tubes (PMTs) required to collect the light from each ΔE/E telescope.

The detector identified charges from Z=2 to Z=27 via ΔE vs. E methods (Fig. 2). This figure is a sample of the data recorded by telescope number 8 for 35 through 65 AMeV ^{84}Kr incident on ^{93}Nb in events triggering two detectors in the main ball of the 4π array.

During the first experiment to use this detector (# 93033), a calibration was performed using a secondary beam from the MSU A1200 particle separator. In that calibration, a fragmentation beam was obtained by colliding a 60 AMeV ^{40}Ar beam on a ^{9}Be target at the entrance to the particle separator. Only particles with discrete momenta passed through the A1200 to the ZDD. That fragmentation beam provided 51 distinct data points with charges ranging from Z=1 to Z=18, and energies on the order of 45 AMeV, for the calibration of this detector (Fig. 3). The magnet setting used to obtain these points was Bρ = 1.9744 Tm (B = 0.63607 T).

The calibration points were used as the input to an IMSL, χ^2 fitting routine, through which the best form and parameterization of the response function were identified. The input data consisted of the 51 fragmentation points, the calculated particle punch-in energies for this detector, and several data points at 95 AMeV, to constrain the energy scale.

Two different forms of the response function were initially considered. The first is the form explored by Cebra[2], and the second was a derivative of Birks' energy loss relations [3,4]. Following are the forms and optimized parameterizations of each.

Cebra:

$$\Delta L = 0.7\Delta E^{0.519} Z^{0.279} A^{0.488} \qquad (1)$$

$$L = 0.2E^{1.118} Z^{0.106} A^{-0.597}$$

Birks:

$$\Delta L = 1.059(\Delta E - C\ln(\frac{C + (\Delta E + E)}{C + E})) \qquad (2)$$

$$L = 0.205(E - C\ln(1 + \frac{E}{C})$$

$$C = 4.700A^{0.0}Z^{1.735}$$

The Cebra parameterization was empirically observed to reproduce the curvature of the response lines better than the Birks formulation. For this reason, the Cebra parameterization was used to create the energy tables for the ZDD.

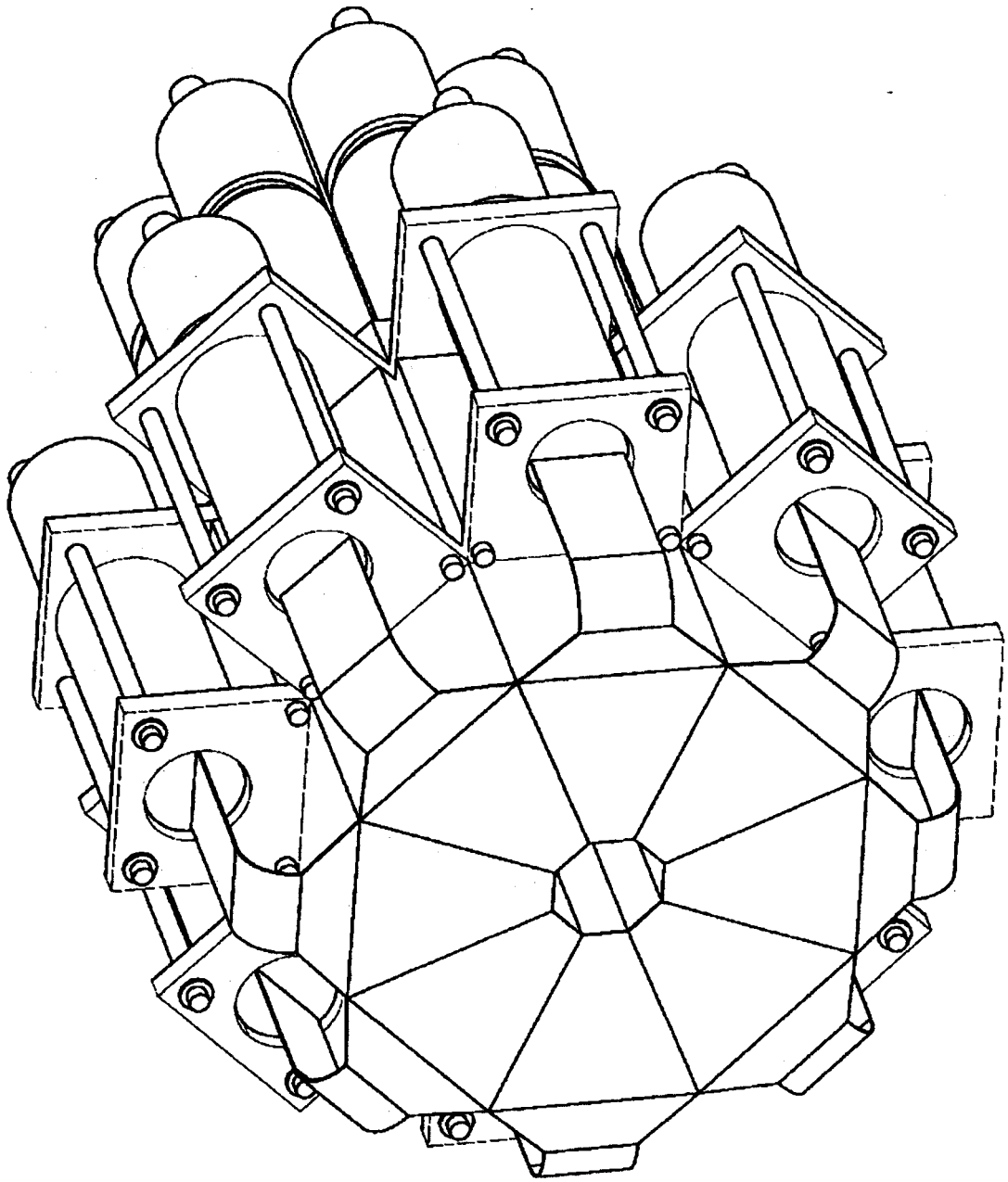

Figure 1: Diagram of the ZDD, showing placement of PMTs and light guides. The beam enters from the lower right.

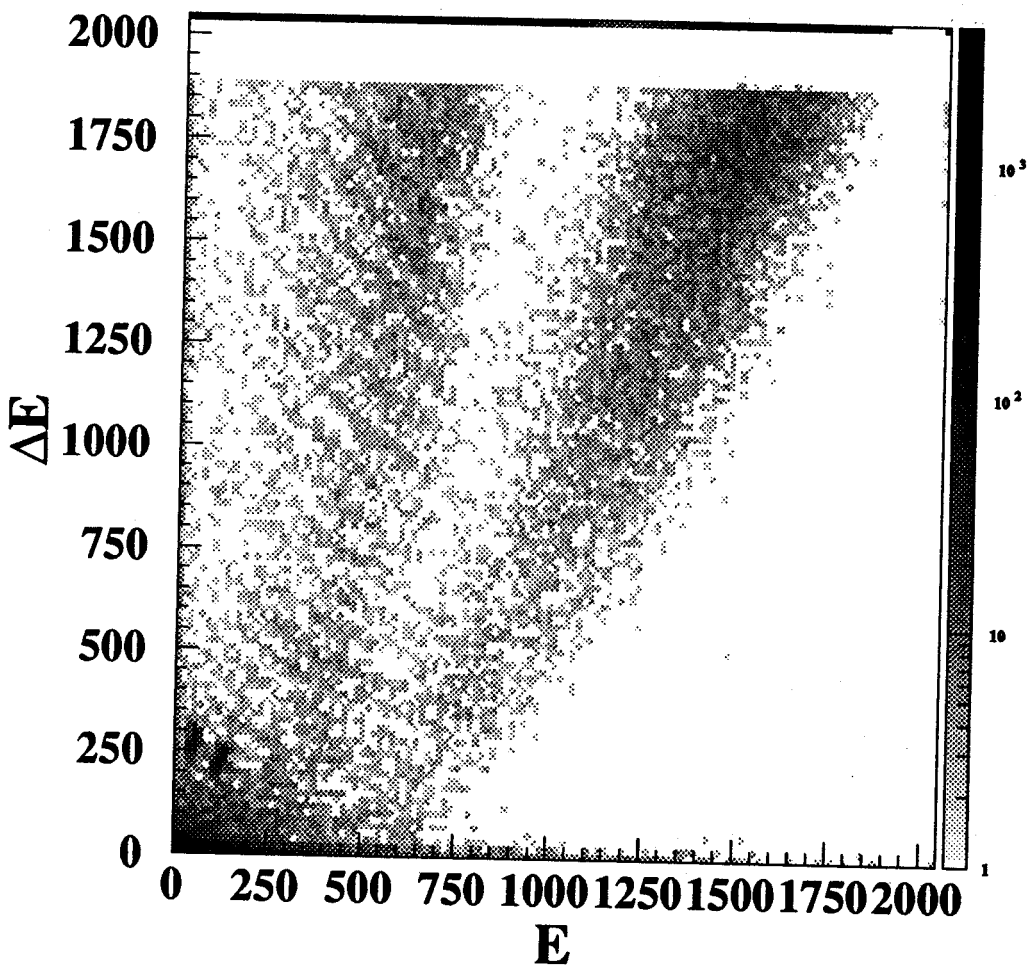

Figure 2: Sample ΔE/E spectrum from segment 8 of the ZDD. Data shown were collected for 4 different beam energies, as described.

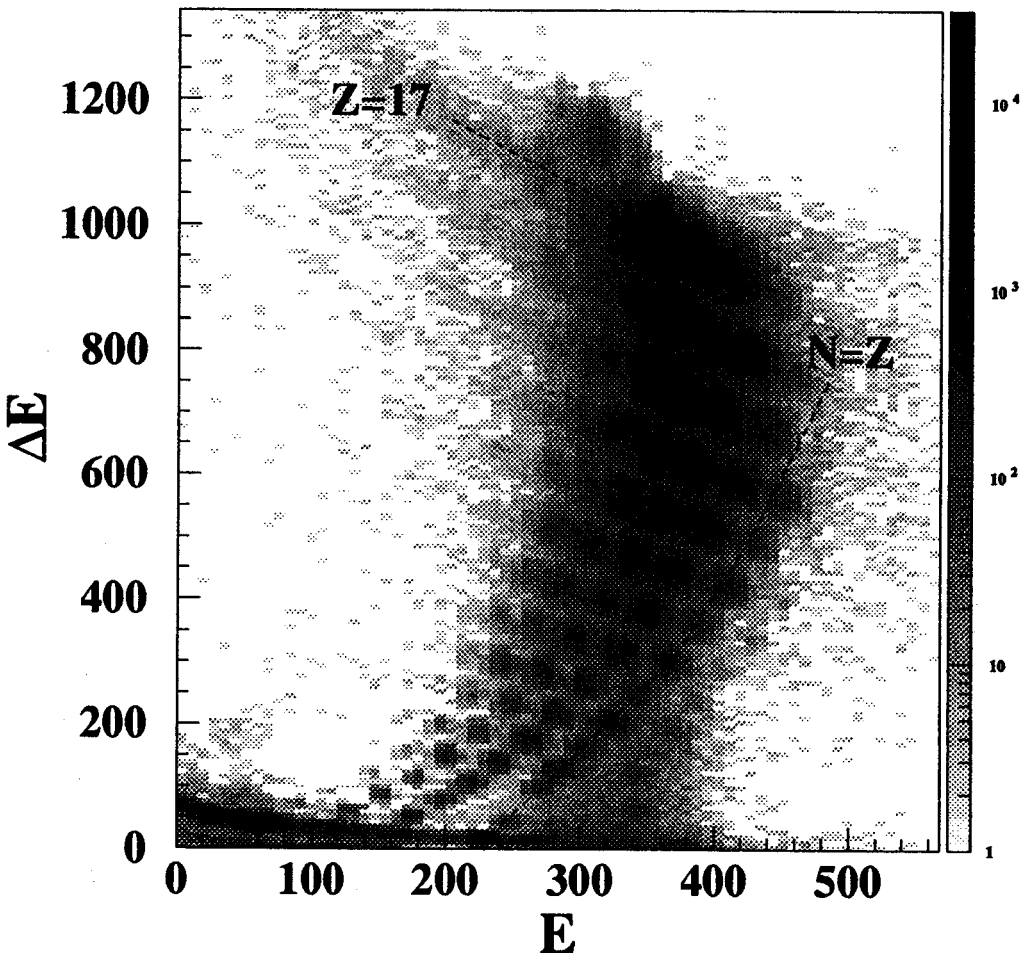

Figure 3: Calibration data from the A1200 fragmentation beam, as recorded in segment 2 of the ZDD.

Analysis of these data is currently in progress, and is directed toward an investigation of the decay of non-compact geometries [5,6]. Preliminary physics tapes have been produced and are being analyzed.

a. Rice University, Houston, TX
b. SUNY - Stony Brook, Stony Brook, NY

References

1. N. T. B. Stone *et al.*, NSCL Annual Report 93, 123 (1993).
2. D. Cebra *et al.*, Nucl. Inst. Meth. A313, 367 (1192).
3. J. B. Birks, The Theory and Practice of Scintillation Counting, Pergamon Press, New York, p.17(1964)
4. C. Pastor *et al.*, Nucl. Inst. Meth. A212, 209-215 (1983).
5. W. Bauer, G.F. Bertsch, and H. Schulz, Phys. Rev. Lett. 69, 1888 (1992).
6. L. G. Moretto, K. Tso, N. Colonna, and G. J. Wozniak, Phys. Rev. Lett. 69, 1884 (1992).

NEUTRON WALLS

P.D. Zecher, A. Galonsky, J.J. Kruse, J. Ottarson, J. Wang, F. Deák,[a] Á. Horvath,[a] K. Ieki,[b] Y. Iwata,[b] Á. Kiss,[a] H. Schelin,[c] and Z. Seres[d]

For a long time there have been experiments at the NSCL (and elsewhere) in which neutrons were detected in a scintillator mounted on a phototube. Neutron velocity was determined from the flight time between production target and scintillator, with target g-rays serving as a calibration. To cleanse the neutron spectrum from time-uncorrelated g-rays, the scintillator was a liquid, a liquid such as NE213 with which one could distinguish neutron from g-ray pulses by pulse shape. One-liter containers of such scintillator performed satisfactorily. In 1991, however, there was an experiment in which the beam was ^{11}Li at an average intensity of 400/sec with about seven disintegrations/sec into ^{9}Li + n + n. To counter the low beam intensity, 54 containers were used. Even so, the statistics were marginal.

To proceed with such experiments, a pair of "neutron walls" has been built. The volume of scintillator is 10 x that in the 54 containers. In a 2-neutron experiment the rate increase can be 10^2. Each wall consists of a stack of 25 glass cells filled with NE213. Each cell is two meters long and has phototubes at its ends. Light from an interaction in the liquid reaches the phototubes via total internal reflection. Recently, the walls were tested with semi-monoenergetic neutrons from the ^{7}Li(p,n) reaction at 30 MeV. The first experiment is scheduled for August. The photo shows one of the walls after the first eight cells had been assembled.

a. Eötvös Lorand University, Budapest, Hungary
b. Rikkyo University, Tokyo, Japan
c. Centro Federal de Educacão Technolocica, Curitiba, Brazil
d. KFKI Research Institute for Particle and Nuclear Physics, Budapest, Hungary

CONSTRUCTION AND TESTING OF A 400 AMP PERSISTENT-CURRENT SWITCH

Jeff Schubert and Henry Blosser

Abstract

Small persistent-current switches carrying up to 100 amps are commercially available. Beyond this current, switches must be custom made and most designs are trade secrets held by private corporations. The Texas Accelerator Center, however, has investigated methods of high current switch building, and they have shared their results with the NSCL, helping us to fabricate a 400 amp persistent-current switch for a .007 henry test coil. To the best of our knowledge, the specifications for similar switches are not published anywhere.

Introduction

Typically, the power supply for a superconducting coil operates at full voltage when raising the current, and thereafter, during d.c. operation, provides only a very small voltage to compensate for the current lead losses. If, after charging, a superconducting shunt is introduced across the leads of the coil, then the current in the magnet will bypass the power supply and current leads, circulating through the coil and shunt continuously. The power supply can then be turned off entirely, eliminating the I^2R heat generated in the current leads. This is persistent-current mode. Small current fluctuations caused by the power supply will also be eliminated, and the current leads themselves may be physically removed to reduce heat conduction into the cryostat [1].

In order to charge the magnet, the switch must be driven normal by a heater. The coil and switch circuit is shown in figure 1. The heater has just enough power to raise the switch above its critical temperature. Soon after the heater is turned off, the switch becomes a superconducting shunt.

Electrical Design

While the magnet is being charged, the switch will act as a resistor in parallel with the coil. Current will be drawn through the resistor creating heat and vaporizing liquid helium. If the coil is charged at a constant rate, the heat energy dissipated may be derived from basic principles.

$$E_R = \frac{E_0 2L}{RT}$$

where E_0 is the magnet's stored energy; L is the magnet's self-inductance; R is the normal resistance of the switch; and T is the time in which the magnet is charged. The size of the switch is directly proportional to R, but if R is too small, then the heat generated when the magnet is charged will be excessive [1].

Most magnets have enough stored energy that if the switch quenches, but the magnet does not, there is a danger of burning the switch. The switch is then protected by putting a resistor (or diode) in parallel with the superconducting shunt. In the event of a switch-quench the current will be shared by the switch and its protection resistor. The combined resistance of the switch and protection resistor is the R that is relevant to calculating the charge losses. In order to add a resistor in parallel with the switch,

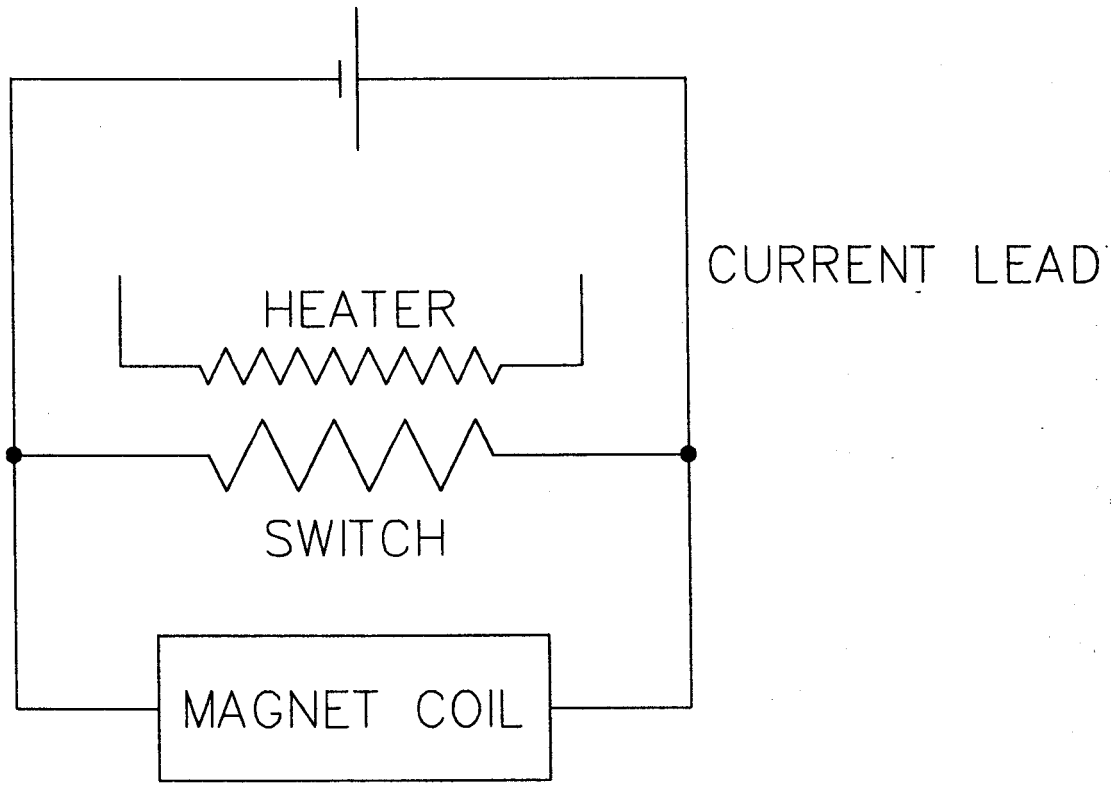

Figure 1: Magnet circuit with persistent-current switch.

without changing the total resistance of the system, the normal resistance of the switch must be increased [1].

For our small test coil (L =.007 H, E_0 =600 joules), a normal resistance of 0.1 Ω would allow us to ramp the coil to 400 amps in .3 seconds while dissipating only 300 joules (enough to boil .1 liter of liquid at 4.2 K.) Because of the small stored energy, we did not worry about the switch being damaged by a quench.

The switch-wire uses 18 filaments of niobium 48% titanium in a resistive copper 10% nickel alloy matrix with a matrix to superconductor ratio of 1.5:1, and a diameter of .030 in. [2]. At a coil current of 400 amps, the maximum field in the switch wire is 0.4 tesla. The manufacturer only provided short sample critical current data for a range from 2 to 6 tesla. Taking the self-field of the wire into account, we extrapolate a critical current of approximately 500 amps at 0.4 T and 4.2 K. The current margin m, defined as $m = (I_c - I_{op})/I_c$ where I_c is the critical current and I_{op} is the operating current, would be 20%. Although such a current margin is generally considered safe, we decided to use two wires in parallel because of our inexperience with this type of wire. (Using two wires also aided in making joints between the switch wire and the much larger coil wire.) With 200 amps in each wire, a maximum field of 0.1 tesla is added to the background field in each wire. With 400 amps in the circuit, the critical current of the switch is then 960 amps. The ratio of operational current to critical current is 42%. At 400 amps the current density in the switch wire is 440 amp/mm^2.

The heater was simply a strand of nichrome-80 resistance wire. A calculation of the amount of power needed to quench the switch wire would be extremely complicated, depending on the nature of the thermal insulation and the geometry of the switch. Based on similar switches built at the Texas Accelerator Center, we used 32 inches of 7 Ω/ft wire yielding a resistance of 18 Ω. Two heaters were provided in case one should burn out during operation.

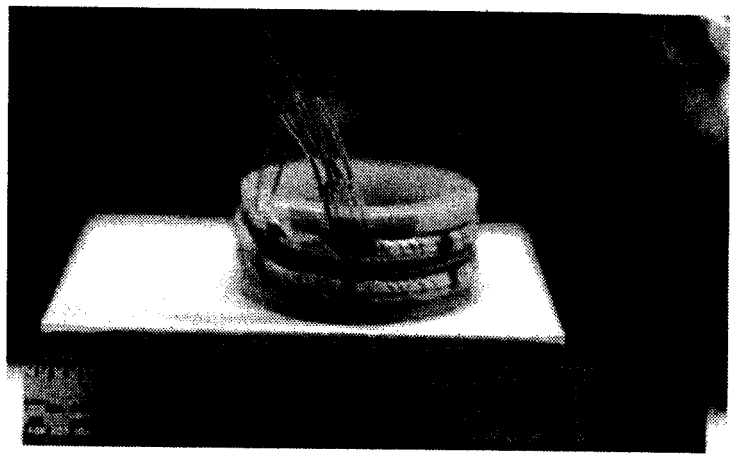

Figure 2: The fully assembled switch, prior to dipping in epoxy. Four leads for the two heaters attach to the switch in front, with the superconducting leads connecting to the left side of the switch.

Mechanical Design and Construction

The switch was assembled in the following manner:

A single woven fiberglass sleeve was slipped over the pair of switch wires for electrical insulation. The insulated wire is then bent double in order to minimize the inductance of the switch.

The nichrome heater wire proved nearly impossible to tin, so instead we attached a piece of copper bus bar wire to each nichrome wire with a dot of silver solder. The heater wires were then wrapped around the insulated switch wire to insure close thermal contact. The switch-wire and heater package was then wound onto a G10 winding form.

The switch was then encased in Epon 815 epoxy [3], which was mixed with G10 sawdust (1% by weight) to protect against crack propagation. First a syringe was used to inject the epoxy under the insulation sleeve. Then the whole switch was dipped in a cup of epoxy and the epoxy was allowed to partially harden before the switch was removed. This resulted in thin coating of epoxy around the entire package.

Too much thermal insulation would result in a switch that was not stable in the superconducting state. Too little thermal insulation would make it impossible for the heater to warm the switch above 10 K to drive it normal. To improve the insulation only when the heater is on, the switch was wrapped in a shroud made of several layers of kapton tape. When the heater is on the helium underneath the shroud should vaporize. If liquid circulation into the shroud is minimal, then the helium vapor will create an additional layer of insulation which disappears when the heater is turned off [5].

Testing

The switch was attached to a test coil made of the same wire as the 8 Tesla magnet [6] and the coil and switch were mounted in the 50 l cryovessel [7] for testing. A heater current of 130 mA, with the two heaters connected in serial, was required to drive the switch normal. The corresponding power was 620

mW. The high power requirement suggests that the switch is too stable, and would have benefitted from a thicker layer of epoxy insulation. It is also possible that the primitive kapton tape shroud allowed too much liquid circulation. (Other switches have used nylon shrouds successfully [5].)

It was not possible to make an accurate measurement of the switching time with our apparatus, however we did determine that both the time required to drive the switch normal and the time for the switch to cool back into the superconducting state are less than 10 seconds.

The switch operated at the design current of 400 amps for a period of 15 hours. The magnet quenched only because the vessel ran out of liquid helium. The power supply was still connected, so the current lead and cables functioned as a dump resistor. Neither switch nor coil showed any signs of damage after the quench. It was not clear whether the coil or the switch quenched first. In future tests we will initiate a quench in the switch with its own heaters (and with the power supply disconnected) to verify that the switch can dissipate the full stored energy of the coil. We also plan to test the switch at 500 amps, the limit of our power supply, and to run the switch for longer periods of time by continuously filling the cryovessel from the 2500 liter dewar.

Superconducting Joints

A persistent-current switch needs to be connected to its magnet with superconducting or nearly superconducting joints. Typically a resistance for the total circuit of $10^{-12}\Omega$ is tolerated. We attempted to make joints following a cold welding method similar to that used at the Tritron, in Munich Germany, to make 236 switches each carrying 40 amps, with a resistance of less than $10^{-15}\Omega$ [8].

Our first attempt resulted in a resistance of approximately $2X10^{-8}\Omega$ at 400 amps, inferred from the rate of current decay. Based on the supposition that the critical current of the joint may be less than that of the wires being joined, we attempted to study the current decay at 40 amps. Unfortunately, the data from the hall probe at this low field was too noisy to clearly distinguish a resistance of $10^{-8}\Omega$ from zero resistance in the time that was available. By continuously filling the cryovessel from the new 2500 liter dewar, we will be able to run for much longer periods of time in the future.

It is not convenient to test a variety of joints with the existing test stand, so a more detailed study of superconducting joint making is left to future investigators. However, we may still investigate the original joints to determine if they function properly at lower currents.

Acknowledgements

We wish to thank Rick Rocha, formerly of the Texas Accelerator Center, for providing the wire and other spare parts, as well as the knowledge required to make this exercise possible.

References

1. M. Wilson, Superconducting Magnets, Oxford University Press (1983).
2. Supercon Inc., Shrewsbury, MA.
3. Shell Chemical Co., Houston, TX.
4. R. Rocha, private communication.
5. J.E.C Williams *et al.*, Rev. Sci. Inst. 52(5), 649 (1981).
6. J. Kim, PhD. thesis, MSU, (1994).
7. J. Kim *et al.*, NSCL Annual Report, 195 (1990).
8. U. Trinks *et al.*, Nucl. Inst. and Meth. A244, 273 (1986).

NSCL MODEL 400 EMBEDDED CONTROLLER

Albert McGilvra, Lynn Foth, and Paul Koblas

Overview

The NSCL Model 400 Controller is a single board computer designed for embedded control applications. It has two 16-bit analog inputs, one 16-bit analog output, 16 digital I/O points, an incremental optical encoder interface, and an RS-485/RS-232 serial port

The Model 400 consists of two major sections: the processing section and the analog subsystem. The processing section is controlled by a Motorola 68332 microprocessor running at 8 MHz. The 68332 also carries out communication with the NSCL control system and runs the application code specific to a piece of equipment. The analog subsystem is controlled by a Motorola 68HC711 microprocessor, also running at 8 MHz.

Processing Section

The processing section contains the 68332 processor, memory, digital I/O, encoder interface, and serial I/O. The analog subsystem handles analog I/O and is described in a separate section below.

Memory consists of a 32K-byte static RAM chip and an EPROM chip that can be 16K, 32K, or 64K-byte. The static RAM is used for data and the EPROM is for code. For program development, the EPROM can be replaced with a static RAM. The code can then be downloaded through the debug port using a background-mode-debugger[1].

The digital I/O is made up of two buffered 8-bit ports. Each port can be programmed as either input or output. Input bits can be programmed to be interrupt lines.

The encoder interface is an IC that reads quadrature output signals from an encoder and counts up or down depending on the relative phase of the quadrature signals. The count is accumulated in a 16-bit register which is read by the 68332.

Serial communication with the Model 400 is normally done via the RS-485 port. However, an RS-232 connection is also provided. The RS-232 connection uses the same serial port on the 68332 as the RS-485 connection, therefore both cannot be used simultaneously.

Analog Subsystem

The analog subsystem consists of three 16-bit analog-to-digital converters (ADC), one 16-bit digital-to-analog converter (DAC), and the 68HC711 processor. Two of the ADC's are used for inputs and one is used to monitor the DAC output for calibration purposes. The 68HC711 processor controls the analog subsystem and communicates with the 68332 via the Serial Peripheral Interface (SPI) link. The SPI is a three-wire master/slave serial link.

The 68HC711 has on-chip EPROM or PROM (depending on which version) that contains its code. It also contains some on-chip RAM for data. The function of the 68HC711 is to offload the processing required for the analog signals from the 68332. It reads, sets, and calibrates the ADC's and DAC through a separate three-wire serial link implemented with digital I/O bits. The DAC setting is received from the 68332 via the SPI link. Likewise, the ADC readings are transmitted to the 68332 via the SPI link.

The ADC's are 24-bit sigma-delta converters. The usable resolution varies with the conversion rate and roll-off frequency, both of which can be programmed in the ADC chip. At the current rate and roll-off we are using the effective resolution of the ADC is about 18-bits. Because of external noise, the effective resolution of the system is about 16-bits. The ADC's can also be programmed to self-calibrate

periodically or on demand. Currently they are programmed to calibrate on demand. To calibrate, the ADC's internally connect their input to ground to obtain a zero data point, then they connect it to the reference voltage to obtain a full-scale data point. These data points are then stored internally and used to calibrate all readings from then on out. Re-calibration is necessary after a power cycle.

The DAC is a 16-bit multiplying DAC which utilizes an external reference. The DAC does not self-calibrate; the 68HC711 takes care of calibration for the DAC. This is accomplished by reading back the DAC voltage with a third ADC. The 68HC711 stores the DAC calibration constants and applies them to all settings from the 68332 before applying the setting to the DAC.

The analog inputs to the Model 400 are differential and contain instrumentation amplifiers so each input can be pin-programmed to have a gain of 1, 100, 200, 500, or 1000. Alternatively, a gain resister can be installed to allow any gain up to 1000. A 10 volt reference is supplied on the analog connector to bias external position pots or whatever else requires a precision bias.

Finally, the 68HC711 has a transmit-only RS-232 debug port which continuously transmits the ADC and DAC values. This port is used only for debugging purposes.

Software

The software of the Model 400 consists of an assembly language program running on the 68HC711 to control the analog subsystem and a C program running on the 68332. The 68HC711 code does not change from one application to another. The 68332 code is designed to be customized for a specific application. It consists of a rudimentary operating system and an Application Program Interface (API).

The operating system handles the RS-485 and SPI interrupt service routines and controls the digital and encoder I/O hardware directly. The API is a set of functions that the user application can call to access and control the analog and digital I/O, get data from the control system, and send data to the control system. The function calls are very simple, so that a user can get an application running with minimal effort.

Summary

The modern superconducting beamlines at NSCL require power supplies with 16-bit accuracy and stability. Also, many of the motion control applications are becoming more and more complex and require more powerful controllers. The primary motivation for designing the Model 400 was to replace the laboratory's 68701 controller for these new and more demanding control applications. The 68701 board design is over ten years old now and has only 2K bytes for program space and 128 bytes for data. The analog subsystem of the 68701 consists of the two 14-bit analog inputs and one 14-bit output.

The 68701 has served the NSCL well as the primary embedded controller for the last decade and will continue to be used in non-critical applications. However, as the need for a faster, more accurate, and more powerful controller became obvious the Model 400 project was initiated to meet that need. Design and testing are now complete and production is underway.

Footnote

1. The background-mode-debugger consists of a special cable and PC software and is available for about $50US from P & E Microsystems (617) 944-7585.

DETERMINATION OF RELATIVE RADIONUCLIDE ABUNDANCES IN NEUTRON ACTIVATED FACILITY PARTS AT THE NSCL

N. Davis[a] and R.M. Ronningen

The disposal of radioactive waste materials presents many problems for the research community. These include expense, storage space, environmental considerations, public health issues and security. Most often the volume of radioactive waste is reduced by segregating the waste into specific radionuclides and concentrating the waste material. However, engineering control of experimental conditions may also be used to limit the production of radioactive waste.

The production of waste materials by accelerator laboratories is unique in that most waste is in the form of activated facility (accelerator, beam-line and experimental apparatus) parts. The purpose of this study was to identify the radionuclides produced in facility parts at the NSCL and to determine their relative abundance. The identification of radionuclides within the activated parts is necessary to determine decay times for storage purposes. But, studies such as this can be used for engineering control over what materials are used for facility parts in high neutron flux environments, so that the amount of waste produced can be minimized.

High resolution gamma ray spectroscopy was used to identify radionuclides in some representative materials used at the NSCL. All gamma ray spectra were obtained using an Ortec high-purity germanium detector, model GEM 90220-P, at 2500 V positive bias, supplied from an Ortec 459 bias supply. For signal conversion, a Canberra Model 2020 amplifier, a Canberra Model 8075 ADC and a PC-based Canberra System 100 multichannel analyzer [1] were used.

The detector was calibrated for energy with a known-nuclide source (NIST standard SRM 4275C-69, September 1, 1988), using photopeaks from well-known gamma rays from the decays of ^{155}Eu, ^{154}Eu, and ^{125}Sb. The photopeak efficiency calibration was performed using the same spectral peaks with their known intensities and uncertainties. The efficiency was determined for a source-to-detector distance of 3.5 inches.

The detector was placed inside a shield constructed of 2 inch-thick lead bricks, with both ends open. Two layers of sheet metal were fitted around the detector sides. The outermost layer was copper, 0.013 inches thick, to shield from lead x-radiation. The innermost layer was cadmium, 0.023 inches thick, for additional shielding from radiation induced within the copper metal. The end plate of the detector was left exposed to the source. Calibrations using the gamma-ray standard, and all data collection, were performed with the sources 2 inches from the lead shield, centered to the detector face, giving an overall source-to-detector distance of 3.5 inches.

Five different materials were analyzed by gamma-ray spectroscopy. These were brass, stainless steel, copper, aluminum, and a collection of miscellany from and including an electrical junction box. The parts were from the NSCL's A1200 radioactive ion beam facility and were neutron-activated during normal accelerator operations. It was assumed that they decayed without further activation from February 7, 1994, when operations ceased to allow an upgrade of the A1200 facility.

The brass samples were two groups of brass fixtures, made from quick-disconnect air-line fittings and threaded tubes. The stainless steel sample was a t-shaped tube having a length of 5.75 inches, a height of 3.25 inches, an inside diameter of 1.38 inches, and outside diameter of 1.44 inches. The copper sample was a group of conflat vacuum seal rings, composed of soft-annealed, oxygen-free high conductivity copper. The aluminum sample was a beam-line vacuum pipe. A "hot spot" on the large aluminum tube was determined with a NaI detector. This region was centered toward the detector face. This activity was possibly from direct beam irradiation, rather than from neutron activation.

calculation yields a representative number of atoms present at the time of spectral analysis. The actual number of atoms present in a given sample was not calculated due to the geometry of these extended sources. To determine a representative number of atoms of each radionuclide present at the time activation ceased, the equation $N = N_0 e^{-\lambda t_d}$, where t_d represents the time of decay. Corrections for peak summing were also performed.

Consistent with the findings of Thomas [4], activated copper contained ^{57}Co, ^{58}Co, ^{54}Mn, ^{56}Co, ^{65}Zn and ^{60}Co; the activated brass contained ^{65}Zn and ^{60}Co; the activated stainless steel contained ^{57}Co, ^{51}Cr, ^{58}Co, ^{54}Mn, ^{65}Zn, ^{60}Co and ^{56}Co. The parts from the electrical junction box contained ^{58}Co, ^{54}Mn, ^{65}Zn and ^{60}Co.

The relative abundance was determined for each radionuclide identified in a given sample. This was calculated by totaling the representative number of atoms of all radionuclides within a sample, dividing the representative number for each radionuclide by the total and multiplying by 100 to obtain a percentage. Results of relative abundance calculations are presented in Table 1.

Neutron activated facility parts in the beam-line present a unique problem in determining their absolute radionuclide abundance, since they are of odd shapes and sizes, and compensations for this and self-absorption must be made. However, relative abundances can be determined. All materials studied here, with the exception of aluminum, contained ^{60}Co as the longest-lived radionuclide ($t_{1/2}$ = 5.3 years). The presence of nuclides with such long half-lives determines storage time and disposal procedures. Future studies on this project will be concerned with developing a method for the determination of absolute radionuclide abundance based upon the geometry of the activated part, the attenuation of the material, and build-up effects.

a. Department of Chemistry, Michigan State University, East Lansing, MI 48824

References

1. Canberra System 100 Software, Canberra Industries, Inc., Meriden, CT.
2. L. Spanier and P. Ekstrom, Computer Code GDISP, version 1.2, July 1990. Department of Nuclear Physics, Solvegatan 14, S-223 62 Lund, Sweden. Data are taken from ENSDF (the Evaluated Nuclear Structure Data File) from 27 February 1990. ENSDF is edited and maintained by the National Nuclear Data Center, Brookhaven National Laboratory, on behalf of the International Network for Nuclear Structure Data Evaluation.
3. E. Browne, and R. Firestone, Table of Radioactive Isotopes, John Wiley & Sons, Inc.(New York), 1986.
4. R.H. Thomas, Health Physics Practices at Research Accelerators, Lawrence Berkeley Laboratory Report LBL-4655, February, 1976.

MEASUREMENTS OF YIELDS OF FISSION PRODUCTS IN THE REACTION OF ^{238}U WITH HIGH-ENERGY p, d AND n BEAMS.

I. Ahmad[a], B. B. Back[a], K. Beyer[a], C. N. Davids[a], J. A. Nolen[a], J. P. Schiffer[a], and R. M. Ronningen

An experiment was performed at the NSCL to determine the yields of neutron-rich fission products in the reaction of ^{238}U with ~100-MeV neutrons, 200-MeV deuterons and 200-MeV protons. Several 1-mm thick ^{238}U foils were irradiated for 100-second intervals and were counted beginning 20 seconds after the end of the irradiation with a 110% Ge detector. Three successive spectra, each with a 40 second period, were accumulated for each sample. For the high-energy neutron irradiation, U foils were placed behind a 12.5 cm long, 2.5 cm diameter Be cylinder, which stopped the 200-MeV deuteron beam and generated 100-MeV neutrons. Arrangements for deuteron irradiation included direct irradiation as well as placing the foils after different lengths (1.2-cm, 2.5-cm, and 3.7-cm) of a 5.0-cm diameter U cylinder. Similar arrangements were also used for proton irradiations. Figure 1 shows a representative gamma-ray spectrum. Yields of many neutron-rich nuclides including ^{90}Kr and ^{132}Sn were determined and these yields were found to be in good agreement with the results of LAHET calculations.

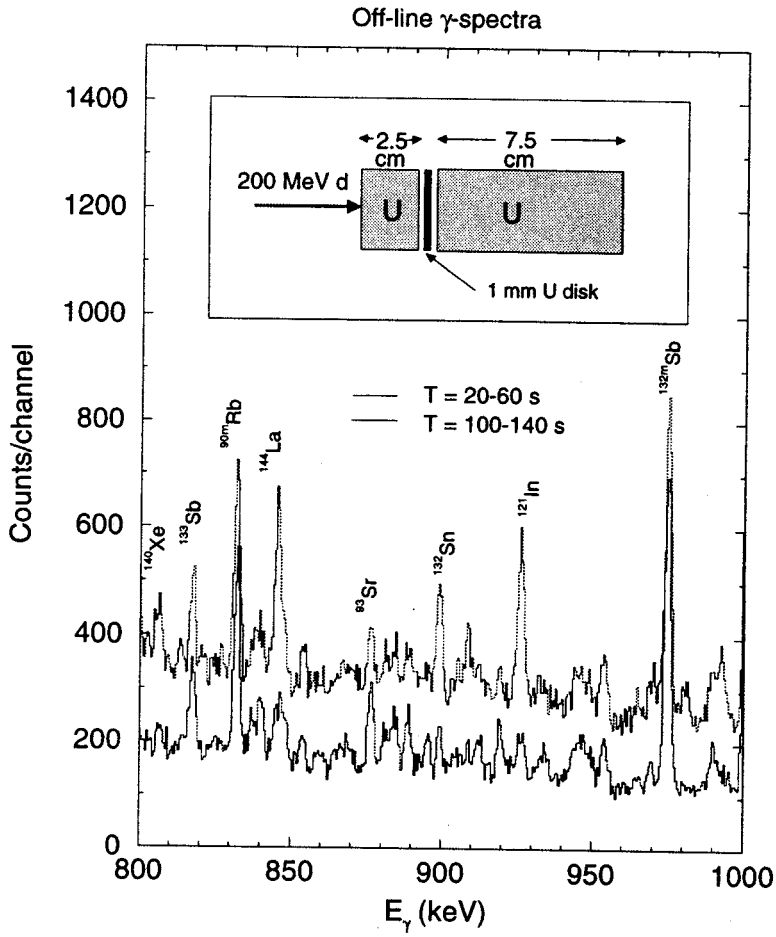

a. Argonne National Laboratory, Argonne, IL 60439-4843, USA